1976

The determination of ultratrace quantities of the toxic metals in biomedical and environmental samples

David Edward Nixon
Iowa State University

The determination of ultratrace quantities of the toxic metals in biomedical and environmental samples

by

David Edward Nixon

A Dissertation Submitted to the
Graduate Faculty in Partial Fulfillment of
The Requirements for the Degree of
DOCTOR OF PHILOSOPHY

Department: Chemistry
Major: Analytical Chemistry

Approved:

Signature was redacted for privacy.

In Charge of Major Work

Signature was redacted for privacy.

For the Major Department

Signature was redacted for privacy.

For the Graduate College

Iowa State University
Ames, Iowa

1976

TABLE OF CONTENTS

LIST OF FIGURES

LIST OF TABLES

I. INTRODUCTION

In our highly industrialized technical society "environmental stress" has become a common phrase. In the past ten years public concern with this "stress" - pollution and work hazards - has steadily increased. Federal agencies such as the Environmental Protection Agency (EPA) have been created to evaluate industrial practices, set standards, and regulate the quantities of organic and heavy metal contaminants released into the environment (1).

The redistribution of Se, Sn, As, Sb, Ge, and Te is of particular interest because they are the toxic nondegradable (2-4) residuals from the burning of fossil fuels (5) and from smelting-refining operations (1,3,4,6). Recent studies have shown that some of these elements (notably As and Se) are emitted as particulates not totally trapped by the electronic precipitators in the stacks of coal-fired electrical generating plants (5). Furthermore, the high incidence of lung cancer near these operations has been correlated with arsenic emissions (1,6). Thus, the high pollution potential for these elements has prompted the enactment of stringent environmental quality requirements (7-10).

In sharp contrast to the known toxicological (3,4,11,12) and suspected carcinogenic properties of a number of these

elements, some of the same elements (Se and Sn) are dietary essentials or possibly essential (As) at very low concentrations (2,11-15). The elements of tremendous importance now are those which possess this "dual role" - toxic and essential - over a narrow concentration range (2,11,13). Some aspects of the biopotency of these elements are discussed very briefly below.

Selenium: Several comprehensive volumes have been dedicated to the description of the biomedical and chemical properties of selenium (16,17). Selenium is readily absorbed, taken up by the red blood cells (18,19), and excreted in the urine (16). In seleniferous areas of the country higher than average dental caries rates (11,16) and lower than normal heart disease (20) and carcinoma (11,21) rates have been reported. Although relatively little is known concerning the mechanism of bioactivity, maximum safe dietary levels of 3 to 4 ppm (11) with a dietary beneficial level of 0.1 ppm (16) have been established.

Tin: Until 1970, tin was considered to be an environmental contaminant; however, it is now considered an essential element with a largely unknown biofunction (15,22). Tin is present in many foods, but the actual intake is highly dependent on the type of diet (11,22). In contrast tin hydride easily enters the blood stream and is extremely toxic (13). Careful experimentation with laboratory

animals has shown that tin is essential at the 1.5 to 2.0 microgram/gram of diet level (14), but liver degeneration has been traced to excessive ingestion (11).

Arsenic: This element has the infamous distinction of being a classic poison. It is rapidly absorbed from food and accumulates in the red blood cells, hair, and nails (13). Urinary excretion is also a pathway of elimination.

A great deal of controversy surrounds the use of arsenic compounds as growth stimulants in animals and as pesticides used on tobacco. Under some conditions arsenic compounds increase tumor and cancer growth whereas, decreases in growth are also observed as conditions change (21).

No normal values of intake have been established because the question of essential intake remains in doubt; however, ingestion of a 100 microgram dose of As_2O_3 will cause severe poisoning (3).

Data collected on As, Se, Sn, and other trace element concentrations in human biofluids and tissues have usually been accumulated on a single element per determination basis. Colorimetric, fluorometric, atomic absorption spectrometric, and electrochemical methods (16,23,24) have been used for the determination of these elements in biological materials in a sequential manner. These techniques have been employed successfully for the detection of short term overexposures to these toxic elements. Beyond these gross effects more

subtle antagonistic and synergistic relationships have been uncovered by analyzing specimens on a simultaneous multi-element basis.

Although spectrographic, neutron activation, X-ray fluorescence, and spark source mass spectrometric techniques have been used for the simultaneous determination of the elements in biosamples (23), precision, sensitivity, accuracy, rapidity or simplicity of sample preparation and analysis may be only marginal at the expected natural concentrations. For example, typical neutron activation analysis procedures for the determination of selenium often call for the irradiation of samples for 20 hours to 14 days followed by a "cooling" period of up to 7 days for the short-lived nuclei to disappear before the actual analysis can proceed (25).

In contrast to the techniques discussed above, the inductively coupled plasma-atomic emission spectroscopic technique (ICP-AES) has recently been shown to produce greater powers of detection for many elements (26-28). The combination of an ICP with a direct reading polychromator (DRP) (29,30) offers the attractive possibility of performing rapid, sensitive, precise determination on a multielement basis.

Explorations on the use of an inductively coupled plasma as an excitation source for analytical spectroscopy were pioneered independently in the United Kingdom (31-33) and at the Ames Laboratory-USERDA (34-38).

A schematic diagram of the complete plasma configuration, including the assembly of concentric quartz tubes (a), argon flow patterns (b and c), and load coil (d) is shown in Figure 1. The torodial shaped plasma (e) is initiated in the following manner. The tangential argon plasma support flow (b) is partially ionized with a tesla coil as it enters the concentric quartz tube configuration. The electrons liberated when the argon ionizes couple with the high frequency oscillating magnetic fields induced by the radio frequency current flowing in the load coil. The accelerated electrons cause additional ionization and the ions and electrons formed flow in closed annular paths (eddy currents) inside the quartz tube. Because the induced magnetic fields are time-varying in their strength and direction, the electrons and ions are accelerated on each half cycle. Joule heating results from the resistance to the flow of the electrons and ions. The foregoing step by step process occurs almost instantaneously and the plasma, once formed, is sustained and thermally isolated from the quartz tube walls by the tangentially introduced argon plasma support flow (b). In addition to this tangential stabilization flow of argon, a lower velocity laminar flow (c) of 1 ℓ/min transports the sample aerosol through the central tube for effective injection into the axial channel of the plasma where the aerosol experiences a high temperature.

Figure 1. Complete plasma configuration

(a) Concentric quartz tubes;
(b) Argon plasma support flow;
(c) Aerosol carrier argon flow;
(d) load coil;
(e) Torodial shaped plasma

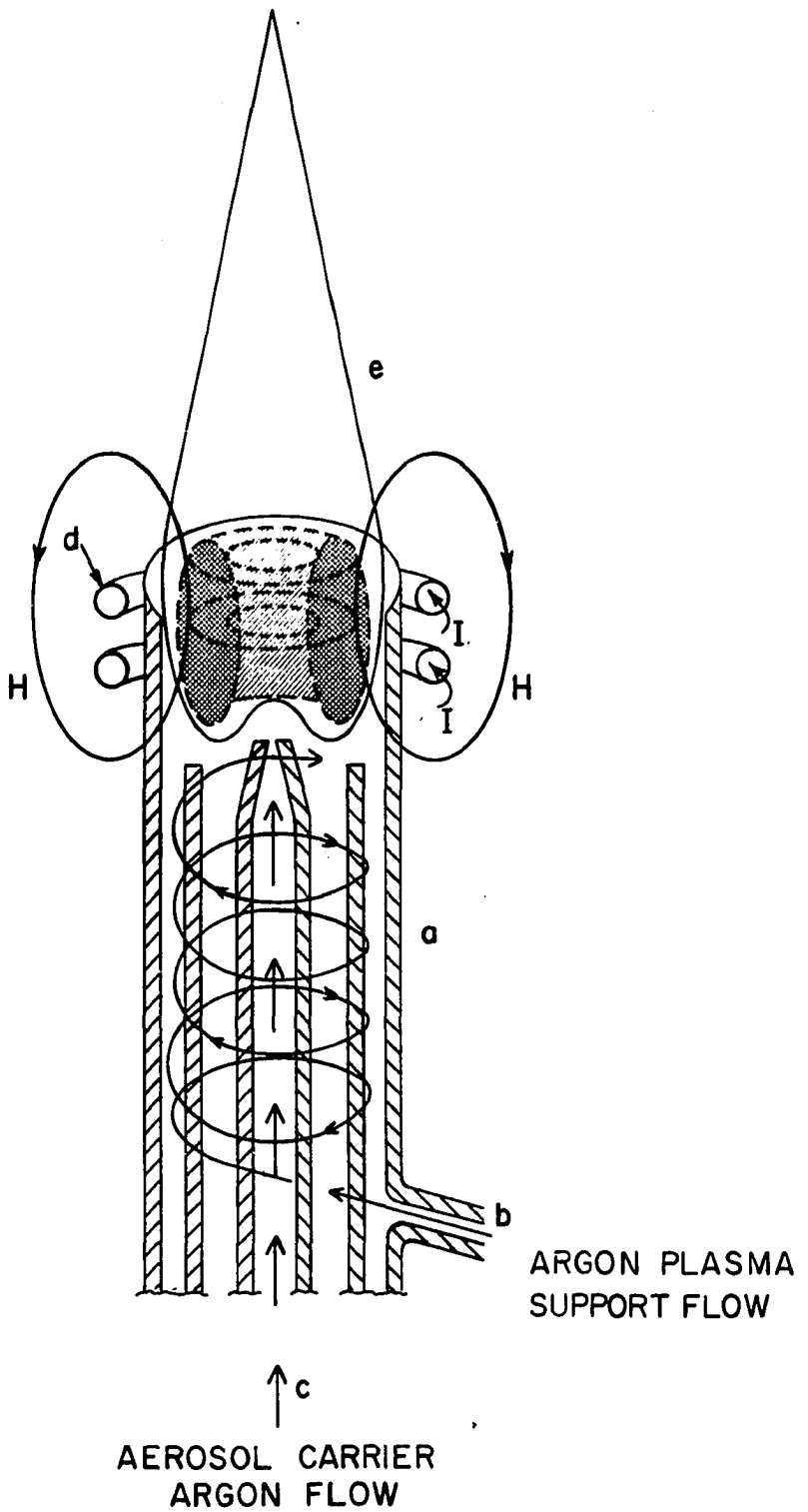
e
d
H
H
I
I
a
b
ARGON PLASMA
SUPPORT FLOW
c
AEROSOL CARRIER
ARGON FLOW

Recognition that the ICP would be a nearly ideal excitation source for the spectroscopic determination of elements is based on the following experimentally observed characteristics of the plasma (39).

1. The analyte emission is confined to a narrow axial channel surrounded by argon having a high gas temperature.
2. Emission from analytes is usually observed above the atomization zone in a relatively constant temperature region (40).
3. The observation of the free atoms or ions confined to the narrow axial channel results in linear analytical curves over 4 to 5 orders of magnitude in concentration.
4. The emission from a large number of analytes can be observed and recorded simultaneously at high powers of detection under one set of experimental parameters.

The conclusion can thus be drawn that the determination of analytes occurring at ultratrace concentrations in a wide variety of samples should be possible in conjunction with a conventional medium resolution spectrometer. Furthermore, the same determinations should be possible on a simultaneous multielement basis by employing a direct reading polychromator (DRP).

The applicability of an inductively coupled plasma-simultaneous multielement analysis (ICP-SMEA) system for the determination of trace constituents in biological and biomedical samples has recently been demonstrated (27,41,42). However, the determination of elements such as As, Se, Sn, and Ge has largely been neglected because these elements occur naturally in biomedical specimens at very low concentrations. The purpose of this investigation therefore, is to determine the toxic and essential elements (Se and Sn), possibly essential (As), and toxic nonessential elements (Sb, Ge, and Te) in biomedical and environmental samples on a simultaneous basis with the ICP as the excitation source.

II. EXPERIMENTAL FACILITIES

The basic components of an ICP-AES facility are: 1) a radio frequency generator, plasma torch, and coupling arrangement; 2) a sample introduction and gas control system; and 3) either a sequential wavelength or simultaneous multiple wavelength photodetection system. Separate single and multiple channel ICP-AES facilities were used in the course of this work. Descriptions of the systems are outlined below.

A. Single Channel Facility (System 1)

Except for the following modifications, complete details for System 1 are contained in the Appendix.

Power control: The stability of the plasma emission signal is a direct function of the power delivered to the plasma. Because changes in the mains voltage produced fluctuations in the radio frequency power level, a feed-back circuit was added to the generator to maintain a constant forward power to the coupling unit. Typical forward operating power was 1200 W.

Aerosol chamber: The aerosol chamber described in Appendix 1 was replaced with a simple Teflon and glass model (27,43). This chamber reduces the clean-out time between samples (44).

Argon flowrates: The argon plasma support flowrate, formerly called the coolant gas in the Appendix, was 17 ℓ/min and the aerosol flowrate was 1.0 ℓ/min.

Observation height: The plasma emission was viewed at 13 mm above the load coil.

Optical system-spectrometer: A 1:1 image of the plasma was focused (for 250.00 nm) on the entrance slit of the spectrometer by a 16 cm focal length x 5 cm diameter plano-convex, fused quartz lens. Fixed 15 μm entrance and exit slits were used with the entrance slit height masked at 4 mm.

B. Direct Reading Polychromator Facility (System 2)

The experimental facilities and operating conditions of System 2 are outlined in Table I. Further details concerning specific components are delineated below.

High-frequency generator: The Plasma-Therm Corp. generator has provision for either manual or automatic servo-control of the loading and tuning capacitors which allow the system to compensate for changes in the impedance characteristics of plasma. The generator also has provision for automatic control of its output power.

Aerosol generation system: The aerosol generation and delivery systems are identical in both Systems 1 and 2. For completeness, the nebulizer, spray chamber, and torch

Table I. Experimental facilities and operating conditions

Aerosol generator	Pneumatic nebulizer as described by Kniseley, et al. (45), and operated at an argon flow of 1 liter/min. Aerosol fed directly to plasma without desolvation. Average sample aspiration rate, 2.5 ml/min.
Nebulization chamber	Teflon and borosilicate glass approximately 160 mm long, tapering from 30 mm i.d., to about 10 mm i.d., operating angle deviates slightly from horizontal to allow free drainage of excess solution from nebulizer end.
Plasma torch assembly	All of fused quartz construction as described previously (46).
Radiofrequency generator	Plasma-Therm Corp. (Kresson, NJ) Model MN-2500 E generator, 27 MHz, 2500 W rating, normally operated at 1100 W. Load coil, 27 mm i.d., made from 1½ turns of 5 mm o.d. copper tubing.
Gas flows (see Figure 3)	Plasma argon: 15 ℓ/min Auxiliary (optional) plasma argon: 1 ℓ/min only for starting the plasma
Polychromator	Applied Research Laboratories QVAC 127 multichannel direct reading polychromator represented for simplicity in Figure 2 with only four exit slits. The grating, with 2160 lines/mm, is blazed for the 170-215 nm region. The spectrometer is evacuated and covers the wavelength range from 170 to 407 nm.
Observation height of plasma	Torch positioned such that optical axis of polychromator corresponded to a height of 13 mm above the top of the load coil. A 6 mm vertical aperture limited the observation

Table I. Continued

Observation height of plasma (continued)	zone to the region between approximately 10 and 16 mm above the load coil.
Photomultipliers	RCA 1P21, 1P28, or their equivalents.
Signal amplifiers (one per output-channel)	Keithley programable amplifier, Model 18000.
Analog/digital converter	Zeltex Model 7210 12 bit converter.
Minicomputer	Digital Equipment Corp., Model PDP 8/E.
Computer interface system	Heath-Schlumberger Model EU-801E.
Data output	Teletype Model ASR-33, or Remex Model RAF-6375 high speed paper tape punch.
Active filters	Two-pole active filters (Ames Laboratory design).

Figure 2. Schematic diagram of direct reading polychromator for simultaneous multielement determinations

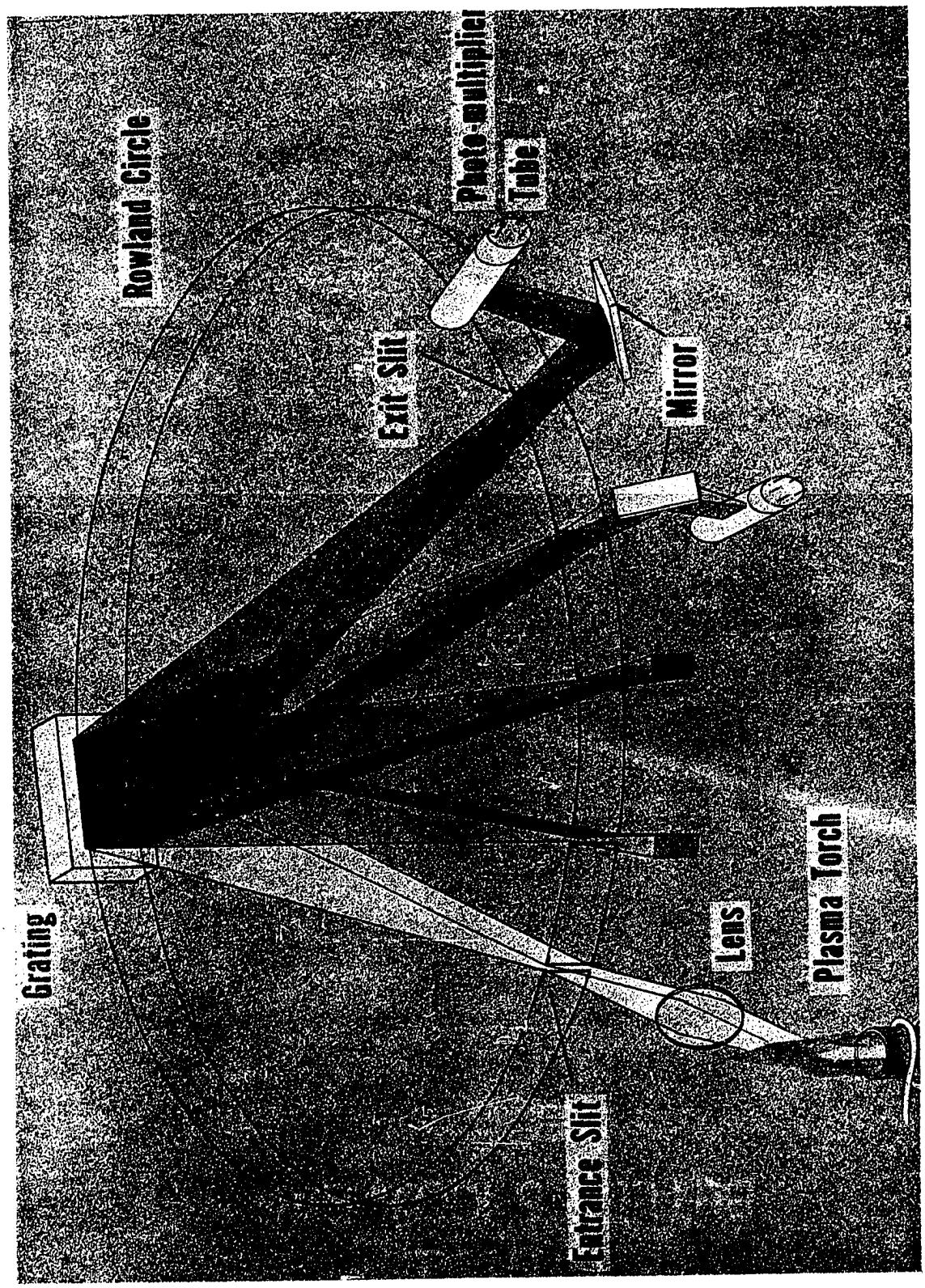
Grating
Rowland Circle
Photo-multiplier Tube
Exit Slit
Mirror
Entrance Slit
Lens
Plasma Torch

assembly are shown in Figure 3. As indicated in the figure, a flared quartz shield is placed over the load coil and around the outer torch tube to provide an insulating barrier between the load coil and the plasma. The probability of an electrical breakdown between the load coil and the plasma is further reduced by connecting the lower winding of the coil to circuit ground.

Gas-flow system: The system for the division and control of gas flows for the inductively-coupled plasma is shown schematically in Figure 4. Argon is delivered from the three-cylinder manifold through two two-stage regulators, the first of which is set at 100 psig; the second at 50 psig. The second regulator considerably reduces the rise in delivery pressure which characteristically accompanies the decrease in tank pressure for most regulators.

Figure 3. Schematic diagram of torch and sample aerosol generation system

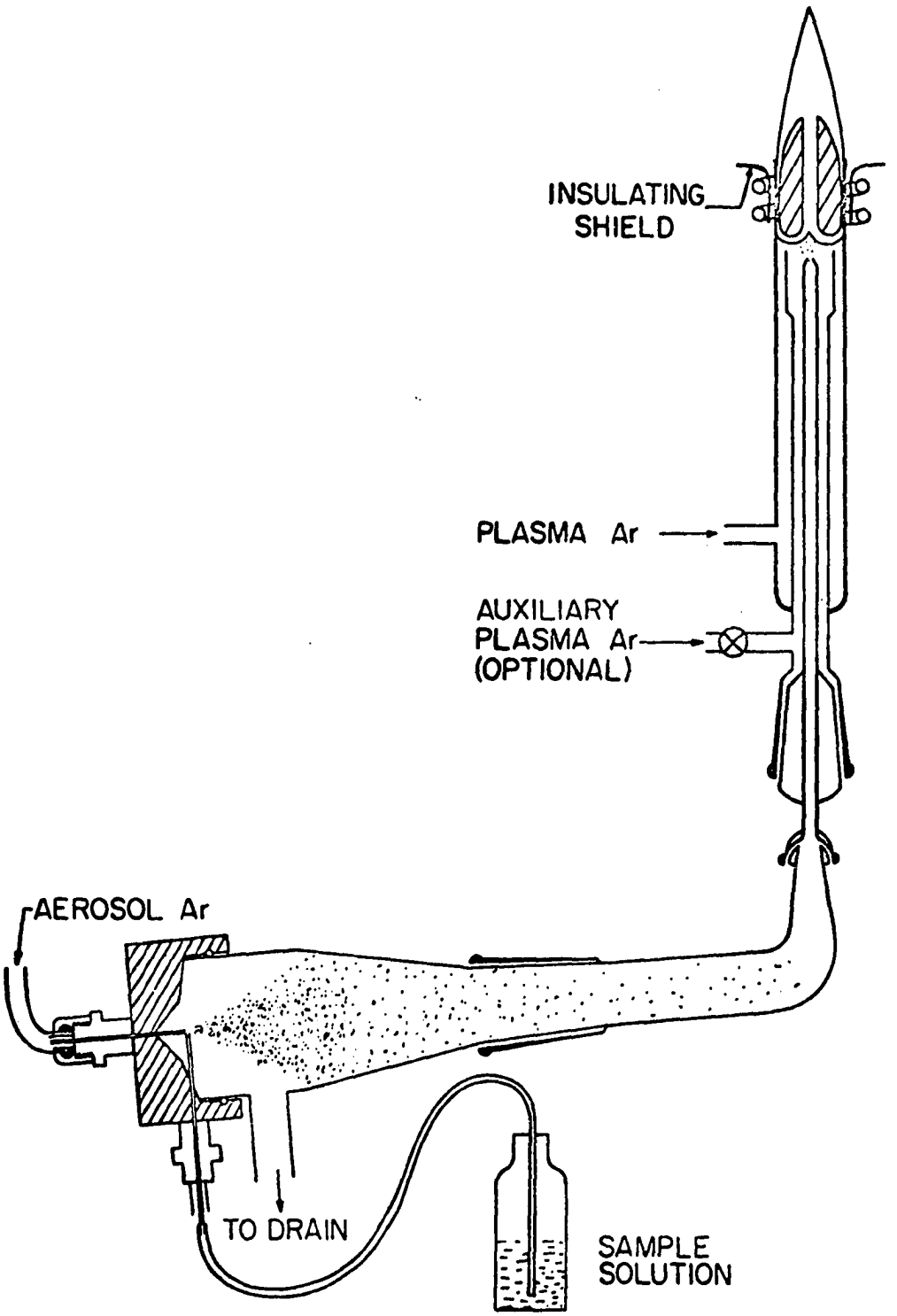
INSULATING SHIELD
PLASMA Ar
AUXILIARY PLASMA Ar (OPTIONAL)
AEROSOL Ar
TO DRAIN
SAMPLE SOLUTION

Figure 4. Block diagram of gas flow regulation system

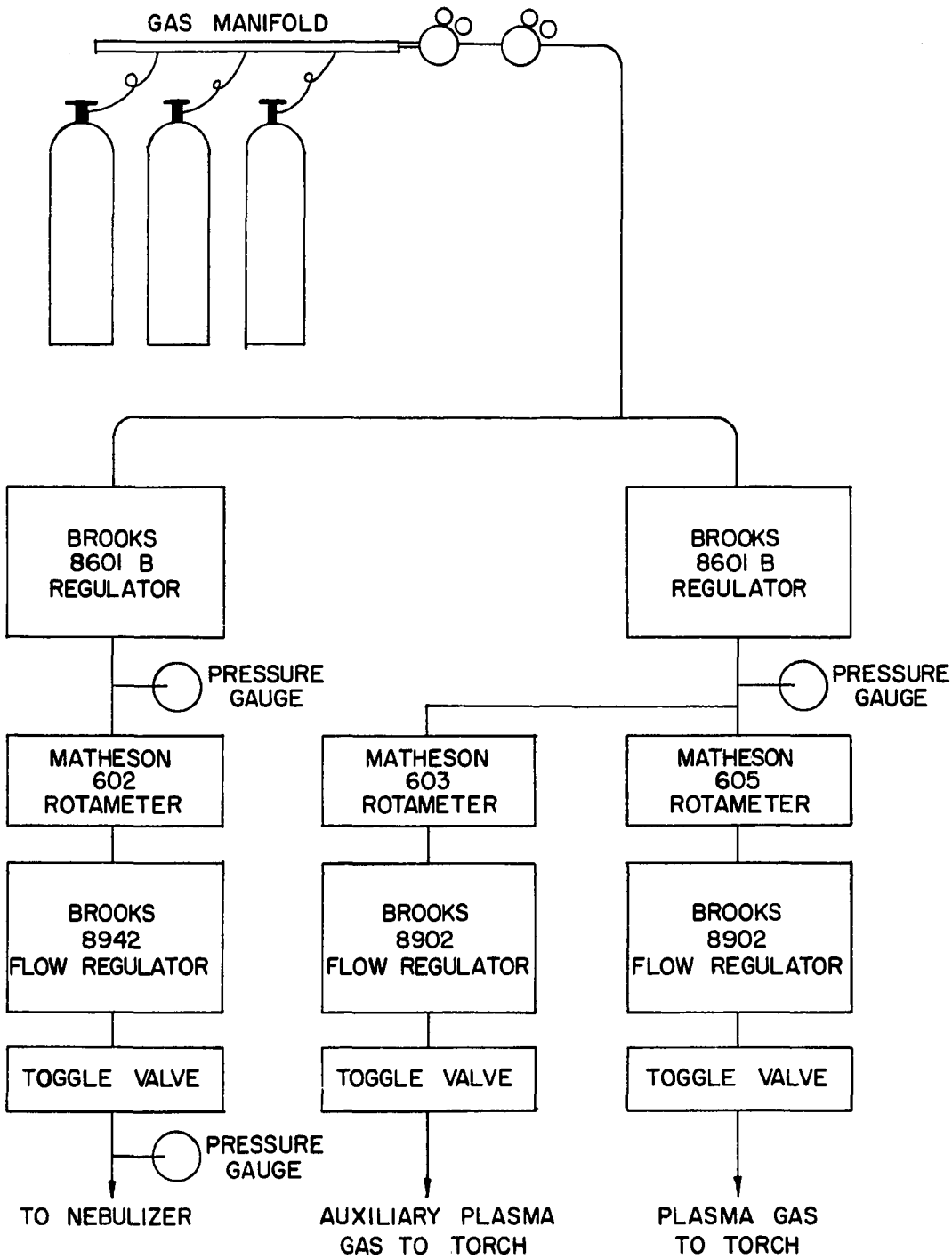
GAS MANIFOLD
BROOKS 8601 B REGULATOR
BROOKS 8601 B REGULATOR
PRESSURE GAUGE
PRESSURE GAUGE
MATHESON 602 ROTAMETER
MATHESON 603 ROTAMETER
MATHESON 605 ROTAMETER
BROOKS 8942 FLOW REGULATOR
BROOKS 8902 FLOW REGULATOR
BROOKS 8902 FLOW REGULATOR
TOGGLE VALVE
TOGGLE VALVE
TOGGLE VALVE
PRESSURE GAUGE
TO NEBULIZER
AUXILIARY PLASMA GAS TO TORCH
PLASMA GAS TO TORCH

III. INDUCTIVELY COUPLED PLASMA-ATOMIC EMISSION SPECTROSCOPY (ICP-AES)

A. Detection Limits

The term detection limit, as used in this investigation, corresponds to the lowest concentration of an analyte that can be detected at the 95% confidence level. A comparison of the normal concentrations of the subject elements in biofluids with the ICP-AES detection limits available at the beginning of this study is presented in Table II. The data in Table II shows that useful quantitative determinations of the listed elements in biofluids were not generally possible. Therefore, the first step in the development of an analytical procedure for the determination of these elements was to investigate the parameters directly affecting the detection limits.

1. Single channel facility

The experimental parameters listed in the lower portion of Table III were varied in order to establish the best detection limits using the single channel facility described in Chapter 2. The conditions listed in Table III, column A, produced the best overall detection limits also listed in column A. These results were obtained sequentially by nebulizing pure water solutions containing one microgram analyte/milliliter of solution into the plasma using

Table II. Comparison of ICP detection limits with normative trace elements concentrations in biofluids[a]

Element	Whole Blood (13)	Blood Plasma (13)	ICP Detection Limits (46)
As	0.49	0.04	0.1
Se	0.27	0.11	0.3
Sn	0.13	0.033	0.3
Ge	--[b]	<0.03	--[b]
Sb	0.0047	0.054	0.2
Te	--	<0.03	0.2

[a]All values listed in terms of µg analyte/ml sample.

[b]Value not listed.

Table III. ICP detection limits and conditions

Elements	Wavelength	(A) Single Channel Facility	(B) Direct Reading Polychromator Facility
As	193.7 nm	0.04[a]	0.03[a]
Se	196.1 nm	0.03	0.02
Sn	303.4 nm	0.15	0.06
Ge	265.1 nm	0.014	0.02
Sb	217.5 nm	0.005	0.01
Te	214.3 nm	0.024	0.08

Experimental Parameters

Forward Power	1200 W	1100 W
Plasma Argon Flow	17 ℓ/min	15 ℓ/min
Aerosol-Carrier Argon Flow	1 ℓ/min	1 ℓ/min
Observation Height (above load coil)	13 mm	13 mm

[a]All values listed in terms of μg analyte/milliliter of solution.

conventional pneumatic solution nebulization (45). The pure water reference blank and analyte emission signals were integrated successively a number of times. The average net analyte signal intensity and twice the standard deviation of the reference blank signals were used to calculate the limit of detection for each element by applying the following equation:

$$\text{detection limit} = \frac{2 \times S \times \text{analyte concentration used}}{\text{average net analyte signal intensity}}$$

Here S equals the standard deviation of the measurements of the reference blank signals. This equation is appropriate because the ICP-AES system has linear intensity response as a function of analyte concentration over several orders of magnitude down to and including the detection limit.

A comparison of the detection limits listed in Table II with those in Table III, Column A, shows that optimization of System 1 parameters produced on the average less than an order of magnitude improvement.

2. Direct reading polychromator (DRP) facility

The ICP-DRP system described in Chapter 2 was used to determine the detection limits listed in Table III, Column B, using the experimental conditions also listed in Column B. The detection limits were calculated in the same manner as above from the net intensities and standard deviations

derived from measurement of 10 successive 20-second integrations of the signals produced by the nebulization of a deionized water reference blank solution and a reference standard containing 1 microgram of each of the analytes per milliliter of solution.

A comparison of the detection limits determined using both facilities (Columns A and B of Table III) shows that the limits of detection are practically identical when the normal experimental error in detection limit measurements (±50% at the detection limit) is considered; therefore, the following conclusion can be stated.

1. Changes in the values of the experimental parameters listed in Table III for either facility will not improve the detection limits by more than a factor of two.
2. Because the natural trace element concentrations in biomedical samples are very near the best ICP detection limits as shown in Table III, it is apparent that at least one order of magnitude improvement in the limits of detection is needed to assure precise analytical determinations. Furthermore, if the biomedical or biological specimen must be digested or dissolved, and/or diluted, the original concentrations of the analytes are decreased by the dilution factor.

For example, it is desirable to dilute serum, plasma or whole blood 1:1 with deionized water to obtain efficient sample nebulization. In this case the analyte concentrations listed in Table II would be halved.

3. Pneumatic nebulizers of the type used here cannot produce the quantity of sample aerosol needed to improve the detection limits by an order of magnitude or more. This is primarily because optimum analytical performance of the plasma is obtained when the nebulizing argon flow is approximately 1 ℓ/min. More sample is transported to the plasma at higher nebulization flow rates, but plasma performance deteriorates. Although colleagues in this laboratory are investigating alternate methods of solution nebulization, including ultrasonic nebulization (47), the research presented here followed a different course.

B. Alternate Approaches

The detection limits for those elements listed in Table III are inferior to the detection limits obtained with the ICP for the metallic elements (26). The reasons for these poor detection limits can be summarized as follows:

1. The excited states of the Group IVA, VA, and VIA elements are difficult to populate because the energy difference between the ground and first excited state of each of the elements is large. Thus the fraction of these atoms that is excited in the plasma is smaller than the corresponding fraction of atoms with lower energy excited states (e.g., transition elements). The smaller fraction of excited atoms produces less analyte emission and correspondingly poorer detection limits.
2. Spectrometers generally employed for analytical studies do not have gratings blazed for the low wavelength spectral region in which the emission from these high energy excited states to the ground state is observed.
3. In addition to the rapidly declining efficiency of most spectrometers in this wavelength region, the transmittance of quartz lens systems and photomultiplier tube windows is also decreasing.
4. Air also absorbs the atomic emission, not allowing the original signal intensity to be observed.

In an attempt to solve some of the problems noted above Kirkbright, et al. (48,49) and Wohlers (50) investigated purely instrumental solutions. They assembled ICP systems specifically designed to improve the powers of detection for the high excitation potential elements.

In the system designed by Kirkbright, et al. (48) a glass manifold containing a fused silica lens was attached to the entrance slit housing of a 1/2-meter spectrometer and extended to within 3.0 cm of the plasma. The spectrometer and manifold were purged with nitrogen to avoid air absorption. Only limited success was realized using this approach. The As and Se detection limits determined using this system were more than a factor of two times poorer than those shown in Table III. Similar results were obtained by Wohlers (50). In his system an evacuated spectrometer and a closed argon filled path from the plasma to the spectrometer entrance slit were employed.

In view of the failures of these purely instrumental approaches, recourse was taken to concentrating these analytes by either physical or chemical means so that an order of magnitude greater density of analyte could be injected into and excited by the ICP. Descriptions of the techniques employed and the results obtained are given below.

IV. ELECTROTHERMAL SAMPLE VAPORIZATION AND ATOMIZATION (ESVA)

A. Introduction

One of the most sensitive contemporary analytical techniques is based on the thermal atomization of microliter volumes of a sample in graphite furnaces (51-61), from graphite (62-70) or tantalum (71-74) filaments, and from platinum or tungsten wire loops (75), followed by the observation of the free atoms by either atomic absorption or fluorescence. Although exceptional relative and absolute powers of detection and acceptable reproducibility have been achieved by a multitude of variations of these atomization systems, this technique is subject to a rather extensive list of experimental constraints. The most important of these are:

1. for many of the systems, critical experimental parameters must be optimized for each element (63, 66-68, 71, 73, 74);
2. reproducibility may be negatively affected by variations in the carbon filament or furnace tube porosity (51, 54, 56, 59, 64, 65, 70);
3. analytical curves may be nonlinear and limited in range of concentration (51, 56, 57, 60-66, 68, 70, 74);

4. background interferences may arise from non-specific absorption and from light scattering caused by incandescent particles produced in the furnace or above the filament (51, 54, 56-59, 61, 64, 65, 68, 74, 75);
5. the observed signals may be affected by inter-element interferences which originate from the recombination or nucleation of the sample after atomization or from incomplete analyte vaporization and dissociation (56-61, 64-67, 69, 71, 73, 74);
6. simultaneous multielement determinations cannot be performed if the free atoms are observed by conventional atomic absorption or fluorescence techniques.

The combination of either furnace or filament vaporization of samples followed by ICP excitation of the vapor offers the attractive possibility of performing ultratrace determinations on a multielement basis on microliter or microgram sized samples. Moreover, the plasma system also offers promise of overcoming the other limitations discussed above. First, since the free atoms are actually generated in the plasma, a single set of parameters should suffice for the vaporization of many types of samples. Second, interelement interferences arising from recombination or nucleation of the vapor above

the filament should be minimized because the plasma subsequently achieves atomization of the vapor cloud. Third, background interference from the filament or furnace tube does not exist. Fourth, analytical curves obtained from the toroidal shaped inductively-coupled plasma are commonly observed to be linear over a concentration range of 4 to 5 orders of magnitude as shown in the Appendix.

In the following sections some preliminary results are presented on the combination of the tantalum filament vaporization (TFV) of samples followed by the inductively-coupled plasma (ICP) excitation.

B. Experimental Facilities and Procedure

1. Apparatus

A block diagram of the overall apparatus is shown in Figure 5. The plasma facility and the spectroscopic apparatus are described in Chapter 2. A sketch of the filament vaporization device is shown in Figure 6. A 0.13 mm thick tantalum filament with dimensions of 37 mm by 10 mm (c) is positioned between two copper post assemblies (d-k) isolated from the aluminum base (m) by means of fired lava spacers (f). The copper posts and the argon gas inlet port (n) are covered with a quartz dome (a), 55 mm o.d. and 35 mm high. Three aluminum tabs (o) press the dome flange against the recessed O-ring (b) to provide a gas-tight seal.

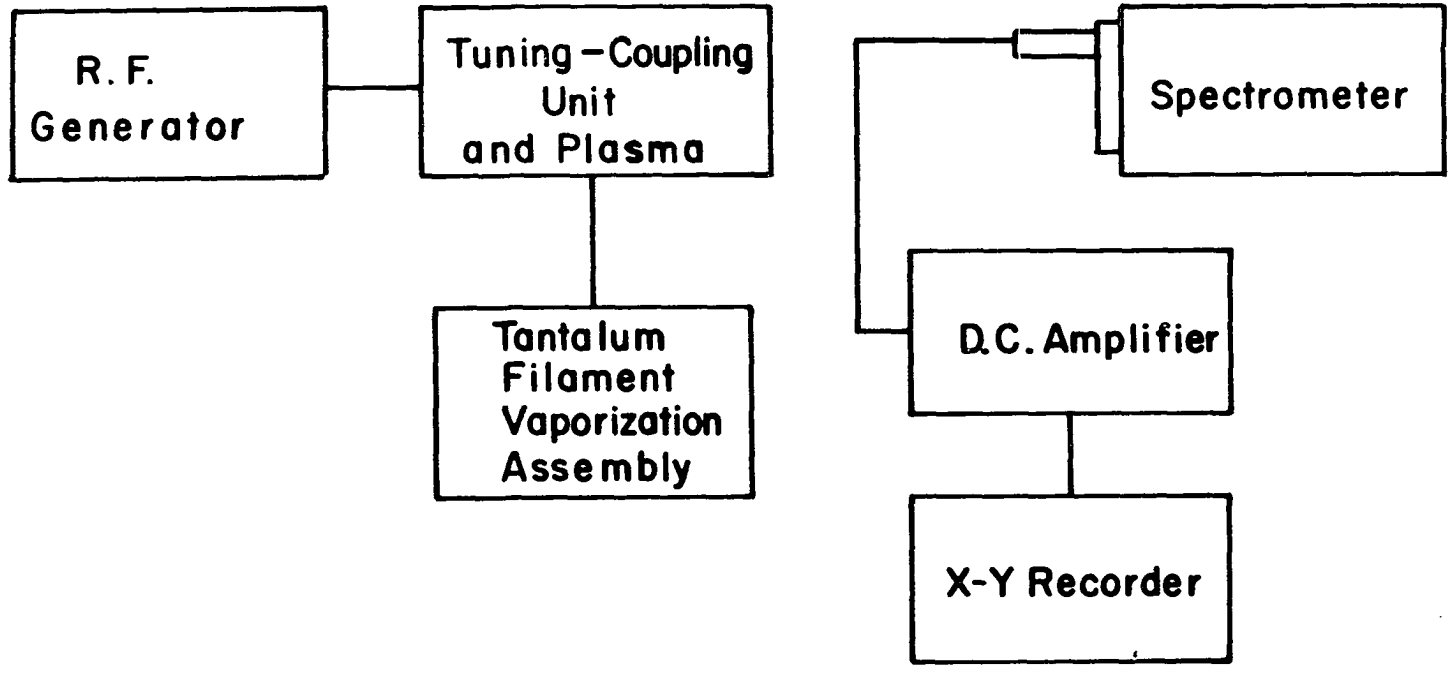

Figure 5. Block diagram of experimental facilities

Figure 6. Tantalum filament vaporization apparatus

(a) quartz dome; (b) O-ring; (c) tantalum filament; (d-k) copper post assembly; (l) O-ring channel; (m) aluminum base; (n) argon gas inlet port; (o) aluminum tabs to seal the dome to the base; (p) sample injection port; (q) port from which argon flows to the torch sample introduction orifice.

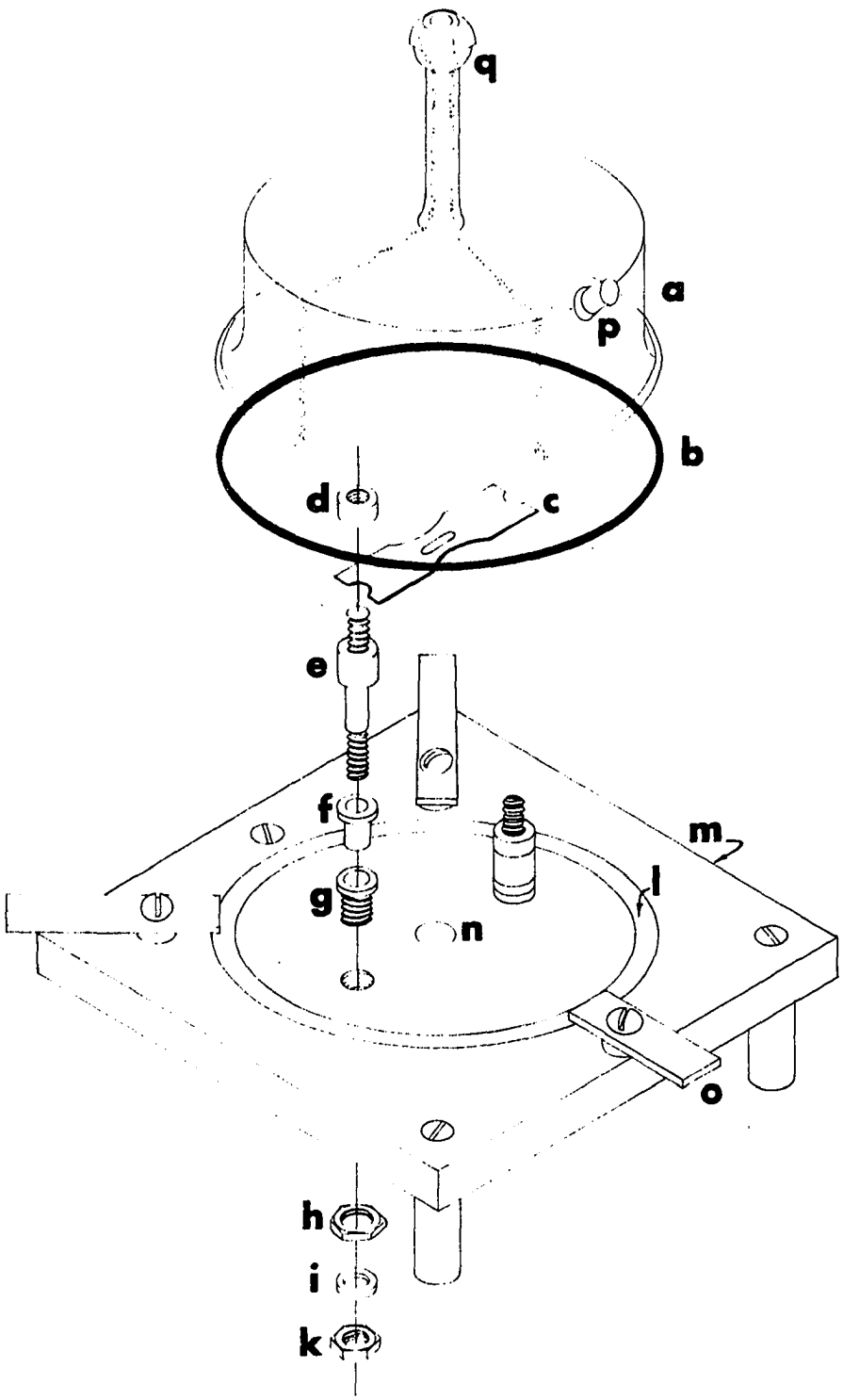
q
a
p
b
d
c
e
f
g
m
l
n
o
h
i
k

Table IV. Operating conditions for the tantalum filament vaporization apparatus

Filament power supply	General electric transformer model 9T51Y6172; 120V primary; 12V secondary; 80°C temperature rise; 0.5 KVA. Transformer input controlled by a Standard Electrical Products Co. variable transformer type F1500BL; 115V input; 0-115V, 2 KVA, 15 amp maximum output.
Tantalum filaments	37 x 10 mm; 0.13 mm thick. Depressions formed with a die; maximum sample volume 200 µl.
Gas flows	Argon at 14.7 l/min proportioned through the plasma and auxiliary plasma tubes to keep the plasma from melting the plasma tube. Argon at 1.2 l/min passes through the filament enclosure to the plasma.
Sample delivery	Hamilton 700 series; model 710; 100 µl capacity with fixed standard needle. Teflon plunger substituted for the original plunger. Eppendorf microliter pipet: Distributed by Brinkman Instruments, Inc.; 50 µl capacity. Standard Eppendorf pipet tips used.
Solutions and sample size	Stock solutions were prepared by dissolving pure metals or reagent grade salts in dilute acid or conductivity water. Samples were conductivity water dilutions of the stock solutions.

The quartz dome is fitted with two ports (p and q) one of which allows the argon gas to flow from the inlet in the base (n) to the sample introduction orifice (q) of the plasma torch shown in the Appendix. The remaining port (p), fitted with a rubber septum, is positioned to allow the delivery of up to 200 µl of sample into a depression in the tantalum filament. The filament is heated by the flow of an electric current obtained from a low voltage, high current transformer controlled by a variable transformer. The operating conditions for the TFV apparatus are described in Table IV.

2. Procedure

After the plasma was generated and stabilized as outlined previously, the argon flowing through the filament chamber to the plasma was adjusted to a flow rate of 1.2 ℓ/min and the spectrometer was set for the desired wavelength. A sample of 1 to 200 microliters was deposited on the filament and a low current (from 10 to 17 amperes) was used to vaporize the water and to ash the deposit. At this point the variable transformer was adjusted to the vaporization setting (∿100A) and a toggle switch was used to rapidly and reproducibly deliver this current to the filament. The filament temperature quickly increased to approximately 1800°C, as determined by optical pyrometer measurements, and the analyte together with the matrix elements were vaporized into the Ar carrier stream.

The photocurrent produced by the emission of the element of interest passing through the plasma was amplified and recorded on an X-Y recorder. Approximately 20 to 30 samples were examined in one hour and the filaments have an average lifetime of 200 to 300 samples.

C. Results and Discussion

Typical detection limits attained with the TFV-ICP system in this study are compared with those obtained by other competitive techniques in Table V. For a majority of the elements studied the TFV-ICP technique provided relative powers of detection which were comparable to the best values reported for ESVA atomic absorption (AAS) or fluorescence (AFS) techniques. A comparison of the TFV-ICP detection limits reported in Table V with the best values so far reported for the introduction of nebulized solution into the plasma shows that the TFV-ICP system is superior by 1 to 2 orders of magnitude. This appears to be the result of the high density of the analyte, already desolvated and vaporized by the filament, momentarily passing through the axial channel of the plasma. The same mechanism is utilized in AAS and AFS when filament vaporization is performed, but for these techniques, the free atoms must be produced at the filament or furnace whereas for the plasma system it is only necessary to vaporize the analytes; the dissociation and

Table V. Detection limits (µg/ml)

Element	TFV-ICP 100 µl samples	Wavelength[a] (nm)	AAS 100 µl samples	AFS	Sample volume (µl) AFS
As	0.01	193.7	0.003(73)	0.25(64)	2[b]
Sb	0.001	231.1	0.001(52)	0.007(52)	30
Se	0.006	196.1	0.007(73)	--[c]	--[c]
Te	0.007	214.3	0.003(73)	--	--
Sn	0.02	317.5	0.025(58)	--	--

[a]Wavelengths used for TFV-ICP detection limits.

[b]Exact volume not stated.

[c]Values not listed.

excitation occur in the plasma. An important fact is that in contrast to the AAS and AFS detection limits, the reported TFV-ICP detection limits were obtained for all the elements under one set of experimental parameters (height of observation in the plasma, filament current, argon flow rates, and plasma forward power settings). This suggests the combination of the TFV-ICP system with a direct reading polychromator described earlier. This combination would thus provide the capability of performing multielement determinations (up to 20 or 30 elements) at the fractional ng level in microliter volumes or microgram samples in less than one minute. Absolute powers of detection were not observed to change significantly for different combinations of sample volume and analyte concentrations. Thus 100 µl volumes of a solution containing 0.0075 µg Sb/ml and 15 µl volumes of a solution containing 0.05 µg Sb/ml yielded comparable absolute detection limits.

An illustration of the precision obtained with the TFV-ICP system is shown in Figure 7. This figure represents the recorder tracings obtained for 15 replicate determinations of Sb at 10 times the detection limit. Typical plasma background signals are shown at (a) and representative Sb emission signals are shown at (b). The signals that appear below the plasma background are caused by the rapid temperature increase of the filament directly in the aerosol carrier gas stream.

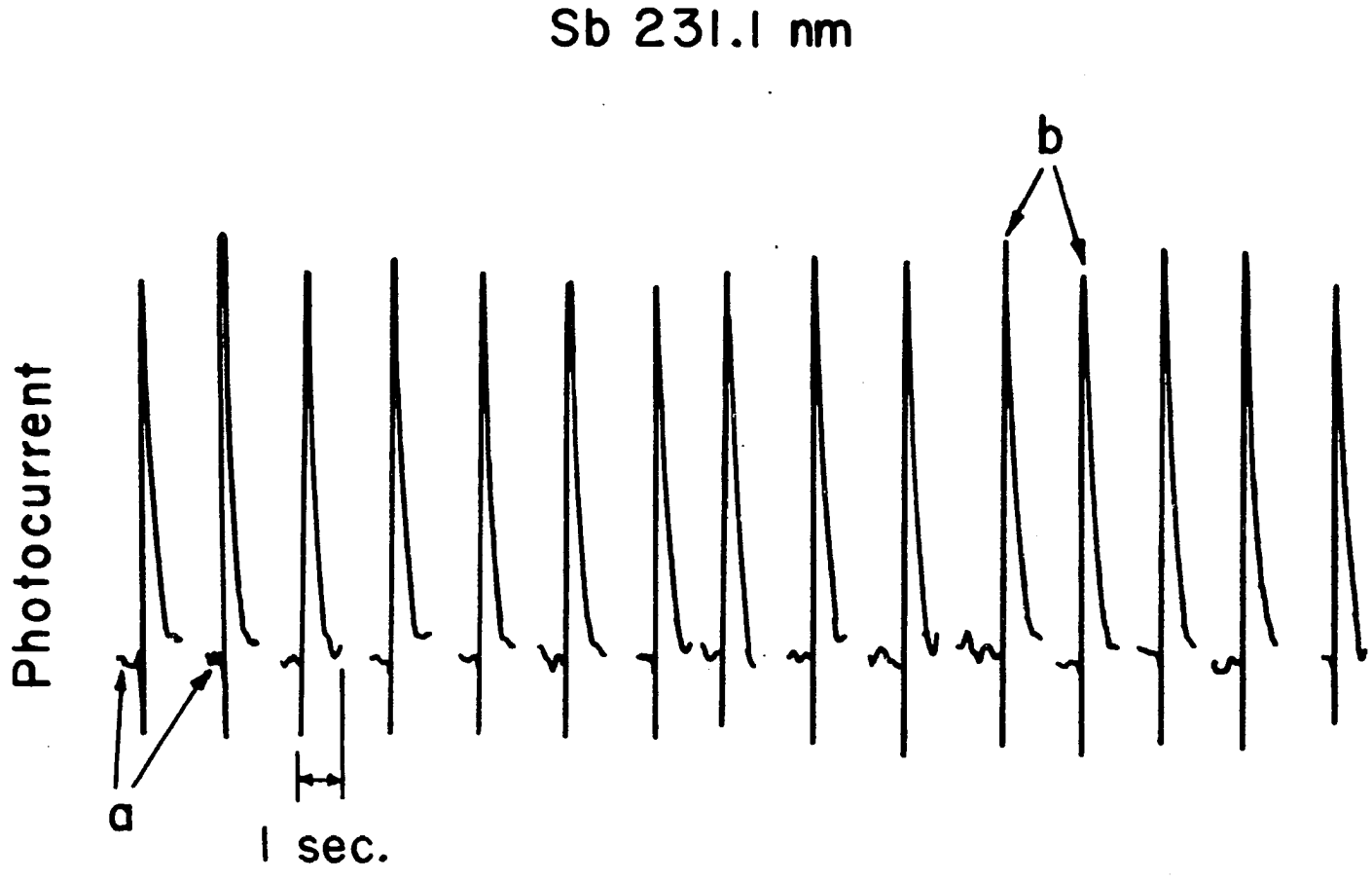

Figure 7. Reproducibility of the TFV-ICP system for 100 µl samples of a solution containing 0.01 µg Sb/ml (1.0×10^{-9} g Sb)

The relative standard deviation of the peak heights, measured from the plasma background to the peak height, is 0.036.

An analytical curve is presented in Figure 8 to demonstrate the applicability of the TFV-ICP system to the analysis of samples with analyte concentrations approaching the detection limit. The curve is linear over two orders of magnitude down to 0.7 ng Te, the detection limit for a 100 µl sample.

To this point, all studies on the electrothermal vaporization (EV)-ICP technique were made on essentially pure water samples containing only nanogram amounts of specific analytes. Before beginning the examination of complex sample materials to determine if unforeseen problems arise, it is appropriate to call attention to an alternate vaporization substrate-pyrolytic graphite.

D. Pyrolytic Graphite Filaments

The technology of employing pyrolytic graphite filaments as substrates for thermal sample vaporization and atomization for atomic absorption spectroscopic determinations experienced rapid development in other laboratories during the course of the present work. Because this substrate possesses some attractive advantages, an evaluation of its merits for use in the EV-ICP technique was undertaken.

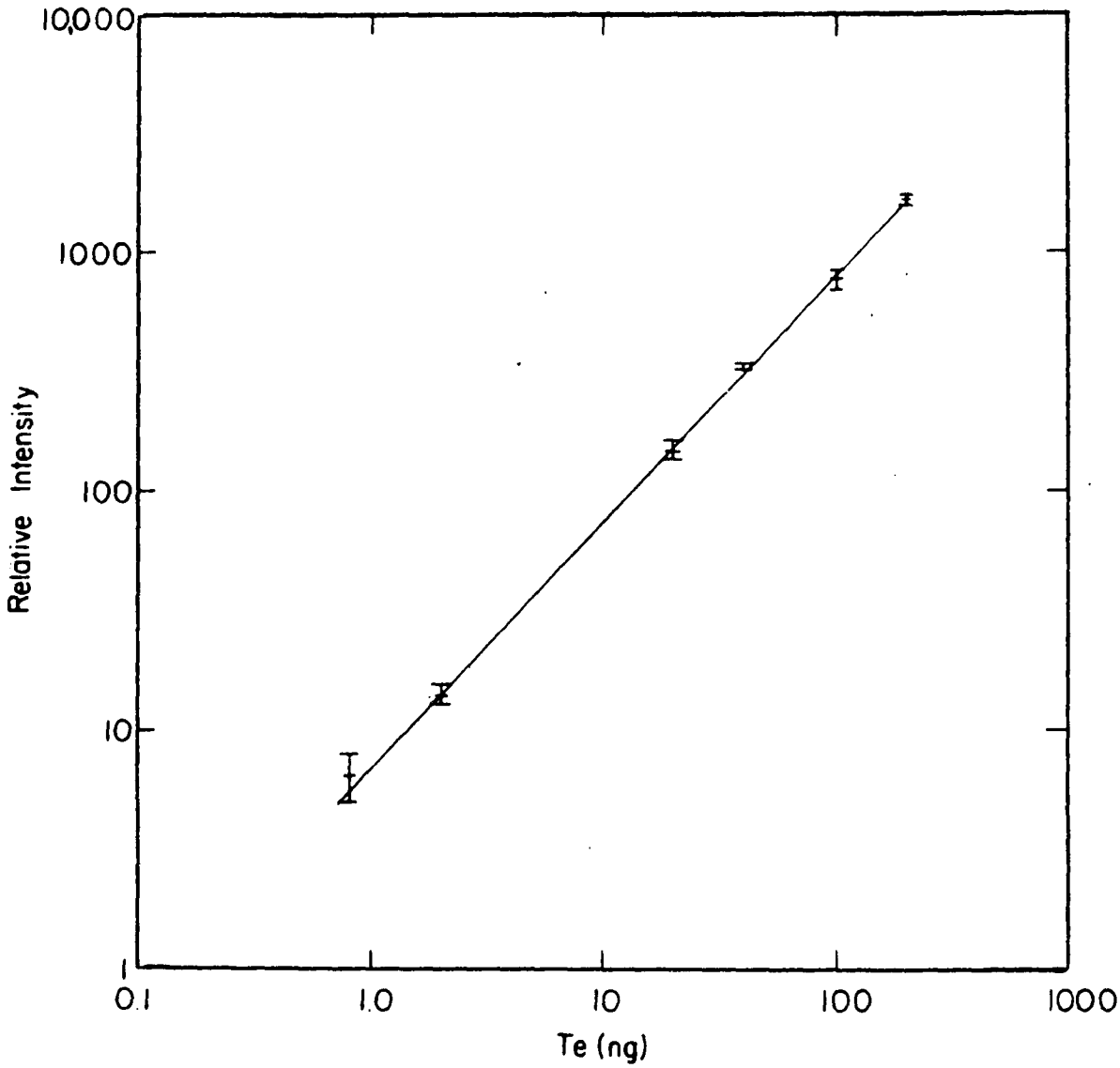

Figure 8. Typical analytical curve for Te in deionized water

Pyrolytic graphite is a material characterized by its high resistance to oxidation, high purity, low gas permeability, and high thermal conductivity (54,76). In addition, aqueous solutions do not soak into this dense, nonporous material (56,65,76-79) and vaporized carbon produces a relatively simple spectrum in the plasma.

Pyrolytically coated filaments measuring 0.254 mm x 9.5 mm x 41.3 mm were provided by Ultra Carbon Corporation, Bay City, MI. These filaments were prepared by coating UT-6 spectrographic grade substrates (density 1.77) with pyrolytics graphite (density 2.28) using a chemical vapor deposition technique (80). The resulting nonwetting, nonporous material can be heated to approximately 3300°C (80) without serious degradation or deformation of the coating.

For the evaluation of these pyrolytic graphite filaments and all subsequent work with tantalum filaments a General Electric model 9T51Y11 transformer rated at 1.0 KVA replaced the 0.5 KVA model. The highest temperature attainable with the 1.0 KVA transformer operated at 112 amperes and 19.7 volts was 2450°C, as measured with an optical pyrometer.

E. Constraints and Limitations of the Thermal Sample Vaporization Technique

The introductory paragraph listed a number of experimental limitations of thermal vaporization-atomization techniques

when the free atoms are measured by atomic absorption or atomic fluorescence. It is appropriate here to examine the constraints which may be encountered when samples such as urine and blood serum are studied by the EV-ICP technique which employs the plasma as the atomization-excitation cell.

1. Physical effects

Changes in the concentration of concomitants (sample constituents other than the analyte) often alter the vaporization and atomization characteristics of the analyte causing the analytical results to be in error. This phenomena has been observed with a number of different vaporization substrates (61, 81-87). Although interelement interferences due to changing concentrations of cation concomitants have been noted in many papers, a more prevalent effect has been the change in the analyte vaporization characteristics as the associated anion is changed (61, 76, 81, 83, 84, 88-92).

2. Refractory compound formation and substrate physical condition

A type of interelement interference that is unique to ESVA techniques results from the interaction of the analyte or concomitant with the filament or furnace. Refractory oxides (90, 93, 94) or intermetallic compounds (89, 90, 94) may be formed, thereby entrapping and immobilizing the analyte. In addition, refractory carbides of analytes or concomitants

may be formed when their salt residues interact with graphite filaments or furnaces at high temperatures (61,88,89,91, 94-96). The interaction of the sample with the filament or furnace is also dependent on the substrate condition (65,76, 77,90).

3. Spectral interferences

A variety of interferences outlined below may result in an analtyical bias unless an accurate correction for their contribution to the total background is made.

a. Atomic spectral interferences Vaporized filament material (95) or concomitant elements may emit strongly at wavelengths coincident or nearly coincident with the analytical lines of the elements of interest.

b. Molecular radiation interferences Concomitants or their decomposition products may produce molecular band emission which overlaps the analyte wavelength. The emission of these molecules usually extends over several nanometers (97).

c. Stray light effects Concomitants may emit very intensely at wavelengths not in the proximity of the analyte line. This emission may reach the analyte detector by reflections or light scattering from the spectrometer walls, optical mountings or grating surface (98,99).

F. Experimental Study of Important Constraints and Limitations

Many of the limitations and constraints outlined above for ESVA-AAS and AFS techniques are not eliminated when electrothermal vaporization (EV) is combined with inductively coupled plasma (ICP) excitation followed by the observation of the atomic emission. Experimental documentation is presented below.

1. Physical effects

The focus of attention in this work was on the effect of anions, especially the chloride ion, on the vaporization characteristics of a typical analyte. When the EV-ICP-AES approach was used for the vaporization and atomization of Pb (76,91), results similar to those reported for various other ESVA techniques were observed. The experimental conditions employed are given below:

Substrate: Tantalum filament

Solutions deposited on substrate:

(a) 2.5 ng of Pb in 25 µl as a solution of $Pb(NO_3)_2$.

(b) 2.5 ng of Pb in 25 µl as a solution of $Pb(NO_3)_2$ plus 25 µl of concentrated HCl.

(c) 25 µl of concentrated HCl.

Drying temperature: Slightly less than 100°C to avoid boiling the deposited solutions.

Vaporization temperature: 1800°C; measured with an optical pyrometer.

Analytical wavelength: Pb 405.7 nm.

No detectable Pb signal was observed for either (a) or (c) whereas a readily measurable signal was recorded for (b). A very likely interpretation of these results is that $Pb(NO_3)_2$ decomposes at 470°C to form PbO (100,101) which itself must be stable at 1800°C because no measurable lead signal was observed. However, the addition of concentrated HCl assures the formation of $PbCl_2$ which readily vaporizes at 950°C (101).

2. Refractory compound formation and substrate physical condition

The experimental observations of vaporization substrate interactions with dried sample deposits were documented using barium as the analyte because it forms a refractory carbide and a thermally stable oxide at temperatures less than 2000°C. Degradation of each substrate type (tantalum and pyrolytic graphite) was observed as the number of heating and cooling cycles increased. The experiments and observations for each substrate type are given below.

a. Tantalum filament Interaction of barium with a tantalum vaporization substrate was observed under the following experimental conditions.

Substrate: Tantalum filament.

Analyte deposited on substrate:

(a) 100 ng of Ba in 10 µl as a solution of $BaCl_2$ in 5% (v/v) HCl.

(b) 1000 ng of Na in 10 µl as a solution of NaCl deposited on filaments previously used for repeated vaporizations of (a).

(c) deposits as in (b). EV-ICP-AES signals observed at two adjacent wavelengths bracketing the Ba emission line.

(d) 10 µl of a solution containing 5% (v/v) HCl deposited on filaments previously used for repeated vaporizations of (a).

Drying temperature: Slightly less than 100°C to avoid boiling the deposited solution.

Vaporization temperature: Approximately 1800°C; measured with an optical pyrometer.

Analytical wavelengths: BaII 455.4 nm for deposits (a), (b), and (c). 455.3 nm and 455.5 nm for deposits (d).

Repeated vaporizations of analyte deposit (a) from a filament previously used for the volatilization of samples containing barium led to nonreproducible signal pulses. Typical results are shown in Figure 9a. Each of the pulse signals displayed in Figure 9a represents the emission of the vaporized analyte as the sample vapor plug from one vaporization cycle traverses the plasma core. The vaporization of NaCl residues (b) from the same filament produced emission peaks at the barium wavelength (Figure 9b), but subsequent vaporizations of NaCl residues (c) with the spectrometer set at wavelengths slightly displaced on either side of the Ba line produced no measurable pulse (see Figure 9c). The foregoing experiment confirmed that the observed pulse signals were produced by barium emission, presumably from Ba residues remaining from prior volatilizations. Although the depositions of NaCl on and its subsequent volatilization from the filament previously used for Ba volatilizations produced strong Ba signals (Figure 9b), no signals were observed when 5% (v/v) solutions of HCl were evaporated on the filament prior to the vaporization process. Thus, whatever the nature of the Ba residue remaining on the filament, the addition of NaCl served to assist in the release of at least part of the residue whereas HCl had no detectable influence. Before attempting to rationalize these findings, the results of another experiment are relevant.

Figure 9. EV-ICP-AES signals produced by the TFV-ICP excitation of the following samples: (a) repeated vaporizations of 100 ng of Ba in 10 µl of solution 5% (v/v) in HCl; (b) 1000 ng of Na in 10 µl as a solution of NaCl; (c) sample (b) at 455.3 nm and 455.5 nm; (d) 10 µl of a solution containing 5% (v/v) HCl in deionized water

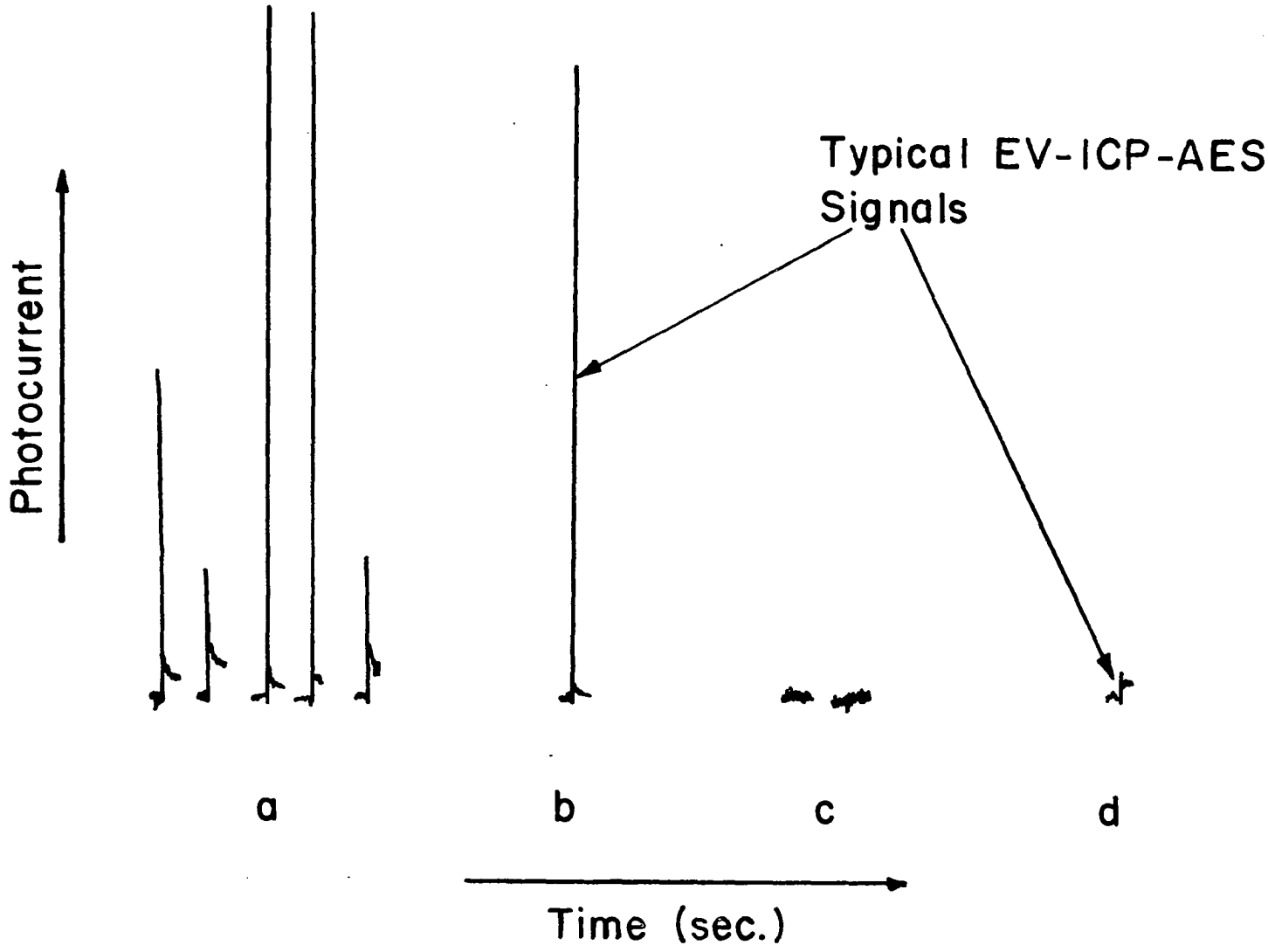
Typical EV-ICP-AES
Signals
Photocurrent
a
b
c
d
Time (sec.)

Substrate: Tantalum filament

(A) Same filament used in the experiment described above.

(B) New filament.

Analyte deposited on substrate:

(a) No sample.

(b) 2300 ng of Na in 10 µl as a solution of NaCl.

(c) 4600 ng of Na in 10 µl as a solution of $NaNO_3$

(d) 100 ng of Ba in 10 µl as a solution of $BaCl_2$ in 5% (v/v) HCl.

Drying temperature: Same as the above experiment.

Vaporization temperature: Same as the above experiment.

Analytical wavelength: BaII 233.5 nm.

The results of experiments (a), (b) and (c) for both the old and fresh filaments (see Figure 10) were not surprising in view of the findings discussed above. The results for experiments (d), however, were strikingly different in the sense that 100 ng Ba deposited and evaporated from an old filament produced no detectable Ba signal whereas a very strong signal pulse was observed when the fresh filament was used. In addition, the vaporization of deposit (b) from the fresh filament (B) after the signal

Figure 10. EV-ICP-AES signals recorded at the BaII 233.5 nm wavelength for deposits vaporized from an old tantalum filament (A) and a new filament (B). The deposited analytes were: (a) no sample; (b) 2300 ng of Na in 10 µl as a solution of NaCl; (c) 4600 ng of Na in 10 µl as a solution of $NaNO_3$; (d) 100 ng of Ba in 10 µl as a solution of $BaCl_2$ in 5% (v/v) HCl

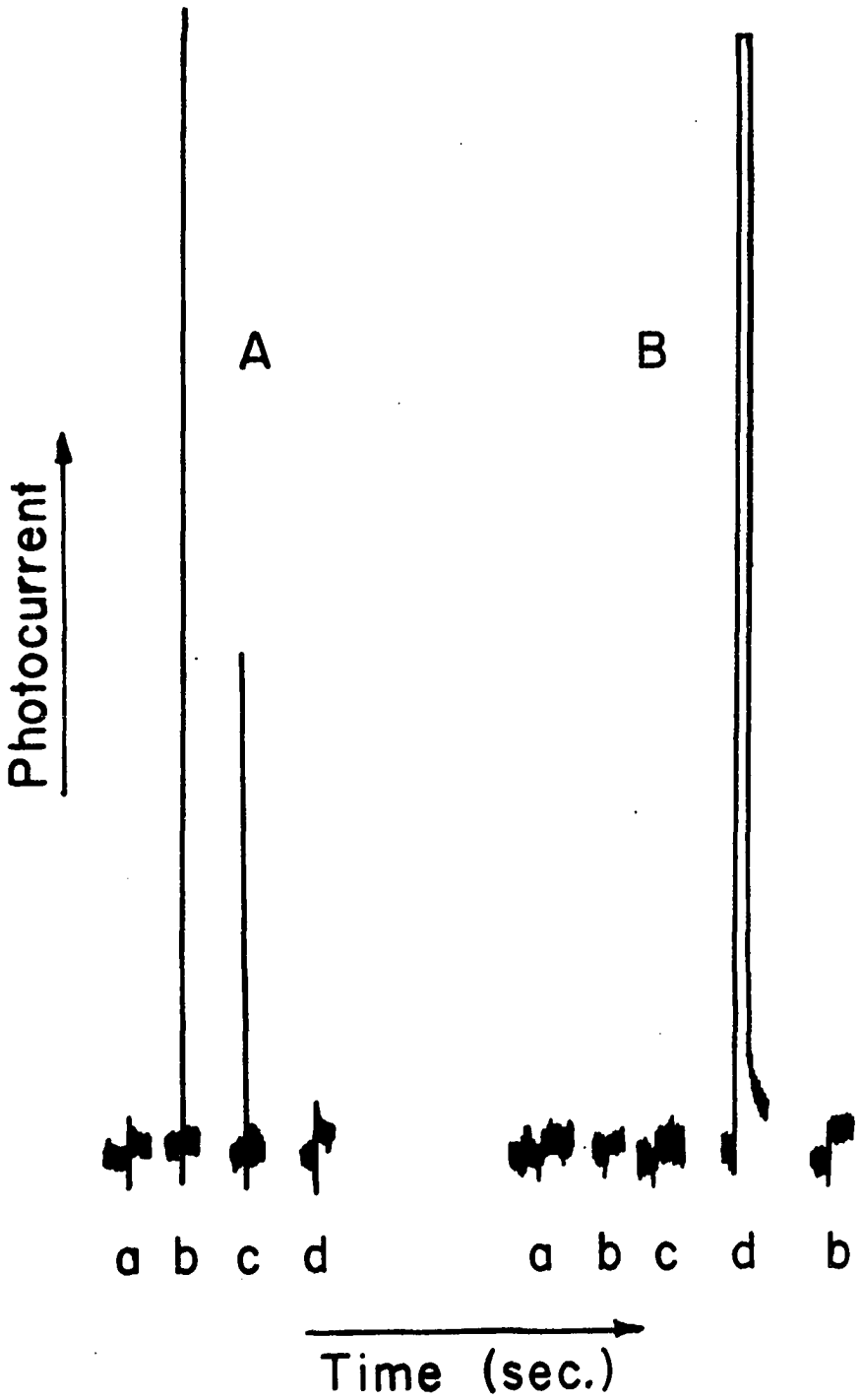
A
B
Photocurrent
a b c d
a b c d b
Time (sec.)

volatilizations (d) (in Figure 10B) produced no measurable signal indicating that a negligible residue remained after only one volatilization.

The set of experiments discussed above suggested that repeated depositions and subsequent volatilizations of barium from filaments that are not replaced between experiments eventually leads to the formation of a refractory compound of barium. Subsequent d.c. carbon arc spectrographic analysis of the dark grey portion of the filament used for the above experiment (Figure 10A) confirmed the presence of approximately 100 ppm of barium. Although it would have been interesting to identify the chemical nature of the compound formed, it was not considered of sufficient importance to warrant further study.

Visual examination of the filament as the number of vaporization cycles increased revealed that the filament progressively turns dark grey and is very brittle when finally replaced. It is known that at higher temperatures N_2, H_2, CO, CO_2, and O_2 react with tantalum to form a dark grey coating (102), and that the hardness, electrical resistance, and density (102) increase. Corresponding changes in the vaporization characteristics of this substrate result (90,94).

The implications of the experiment are important, i.e., the possibility that the behavior of barium is not

unique, the need of using a fresh filament for each sample or each analytical determination, and the time, cost, and inconvenience involved in changing filaments.

b. Pyrolytic graphite Part of the evaluation of pyrolytic graphite as a substrate for the vaporization of barium was accomplished with the following experiment.

Substrate: Pyrolytic graphite filament.

Analyte deposited on substrate:

(a) 20 ng of Ba in 20 µl as a solution of $BaCl_2$ in 5% (v/v) HCl.

(b) no sample.

Drying temperature: Slightly less than 100°C to avoid boiling the deposited solution.

Vaporization temperature: 2450°C; measured with an optical pyrometer.

Analytical wavelengths: BaII 455.4 nm for (a) and (b); 455.5 nm for (a) and (b); BaII 233.5 nm for (a) and (b); 233.6 nm for (a) and (b).

Signal recording device: Tektronix type 545A oscilliscope driven by a Keithly 514 pico-ammeter.

Repeated vaporizations of the dried deposit (a) produced EV-ICP-AES signals at 455.4 nm which were characterized by two maxima (see Figure 11A). Subsequent vaporizations from

Figure 11. Oscilloscope tracings of the ICP signals produced at the 455.4 nm BaII wavelength. Sweep speed was 0.5 sec/cm. A pyrolytic graphite filament was used to vaporize the following samples into the plasma: (A) 20 ng of Ba in 20 µl as a solution of $BaCl_2$ in 5% (v/v) HCl; (B) no sample deposited

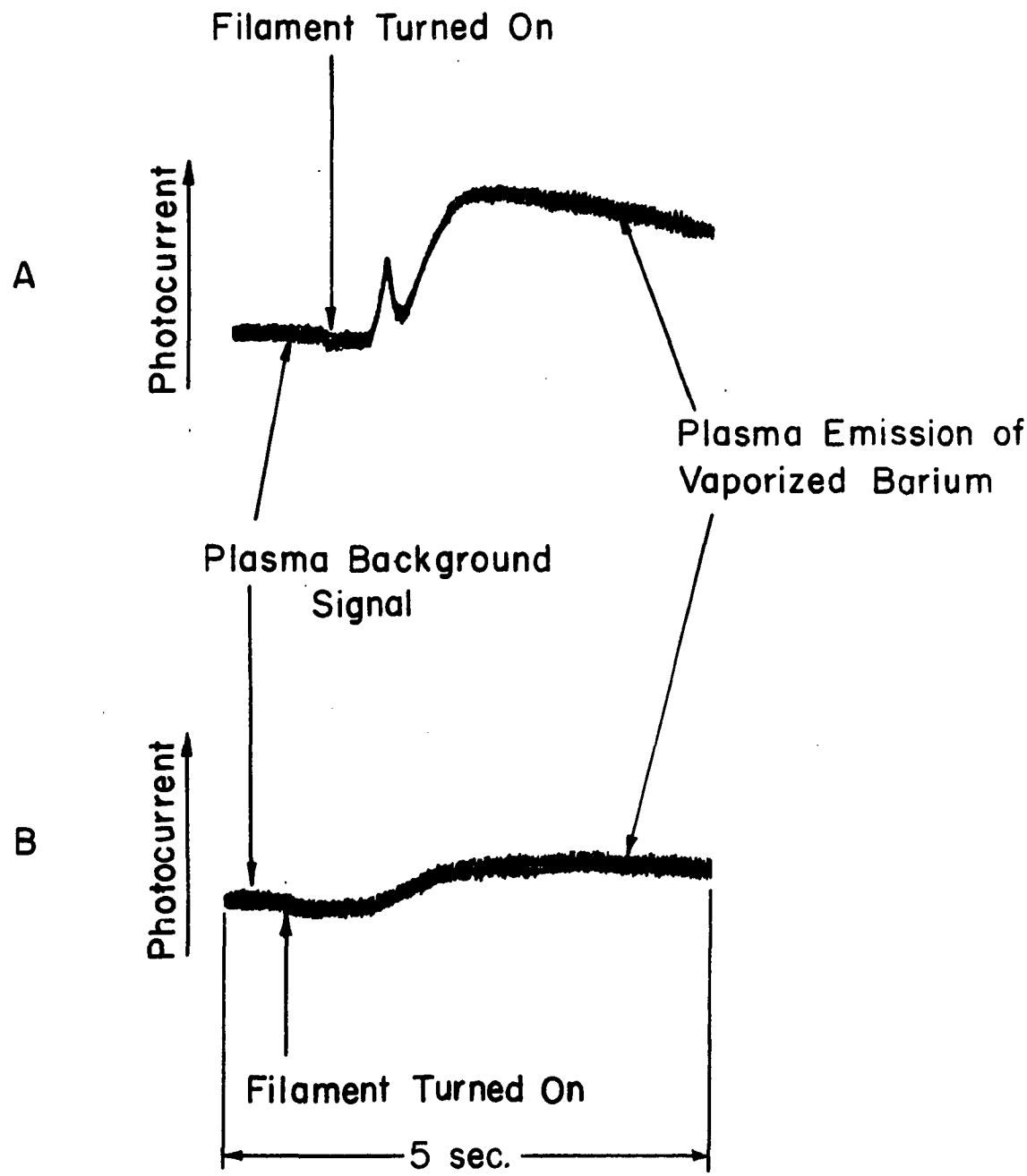
Filament Turned On
A
Photocurrent
Plasma Emission of
Vaporized Barium
Plasma Background
Signal
B
Photocurrent
Filament Turned On
5 sec.

the same filament with no sample present produced emission tracings of the type shown in Figure 11B. Repetition of the same experimental sequence with the spectrometer adjusted to respond to the 233.5 nm barium line gave similar results although neither emission signal (A or B in Figure 11) was observed at a wavelength several tenths of a nanometer from this barium line.

The observation of two barium maxima, the second presumably due to a slower vaporization of a portion of the barium analyte from the substrate, may severely limit the general usefulness of pyrolytic graphite as a vaporization substrate. For quantitative determinations, integration of the total signal pulse may be necessary.

The condition of a pyrolytic graphite filament was also monitored visually as a function of the number of vaporization cycles. After more than 200 vaporizations of sample residues including undiluted urine and concentrated nitric acid, at temperatures ranging from 2000°C to 2450°C, the substrate surface appeared similar to that of a new filament. Microscopic examination at 40 power revealed that the new and used filament surfaces were identical in structure with no apparent residue on the used filament. This suggests that pyrolytic graphite is more resistant to chemical attack than tantalum.

3. Spectral interferences

a. Atomic spectral interferences An illustration of the type of spectral interference encountered in experiments with the tantalum filament is given in Figure 12. The tantalum emission lines identified in (a) (103) also appear in (b) and the TeI 214.28 nm line occurs between two closely spaced TaII lines. The conclusion is that a spectral interference results from the vaporization of tantalum from the filament.

Investigations of the SeI 196.1 nm and SeI 203.9 nm wavelength regions resulted in similar conclusions.

b. Stray radiation and molecular band emission interferences Introduction of samples containing certain inorganic or complex organic concomitants into the plasma often results in molecular band emission (104) and/or stray radiation (98) in addition to analyte emission signals. This is true whether electrothermal vaporization (EV) or solution nebulization (SN) techniques are employed.

Because body fluids such as blood and urine contain varying amounts of organic and inorganic materials from subject to subject and from day to day, it is evident that the signals observed at a particular elemental wavelength may include different intensity contributions which are not related to the analyte concentrations. Results of the experiment described below clearly illustrate the problem.

Figure 12. Wavelength scans from 213.5 nm to 215.0 nm showing the plasma emission of the following: (a) 2500 µg Ta/ml of solution nebulized into the plasma; (b) vapor from the tantalum filament operated at 2200 °C; (c) 4 µg Te/ml of solution nebulized into the plasma

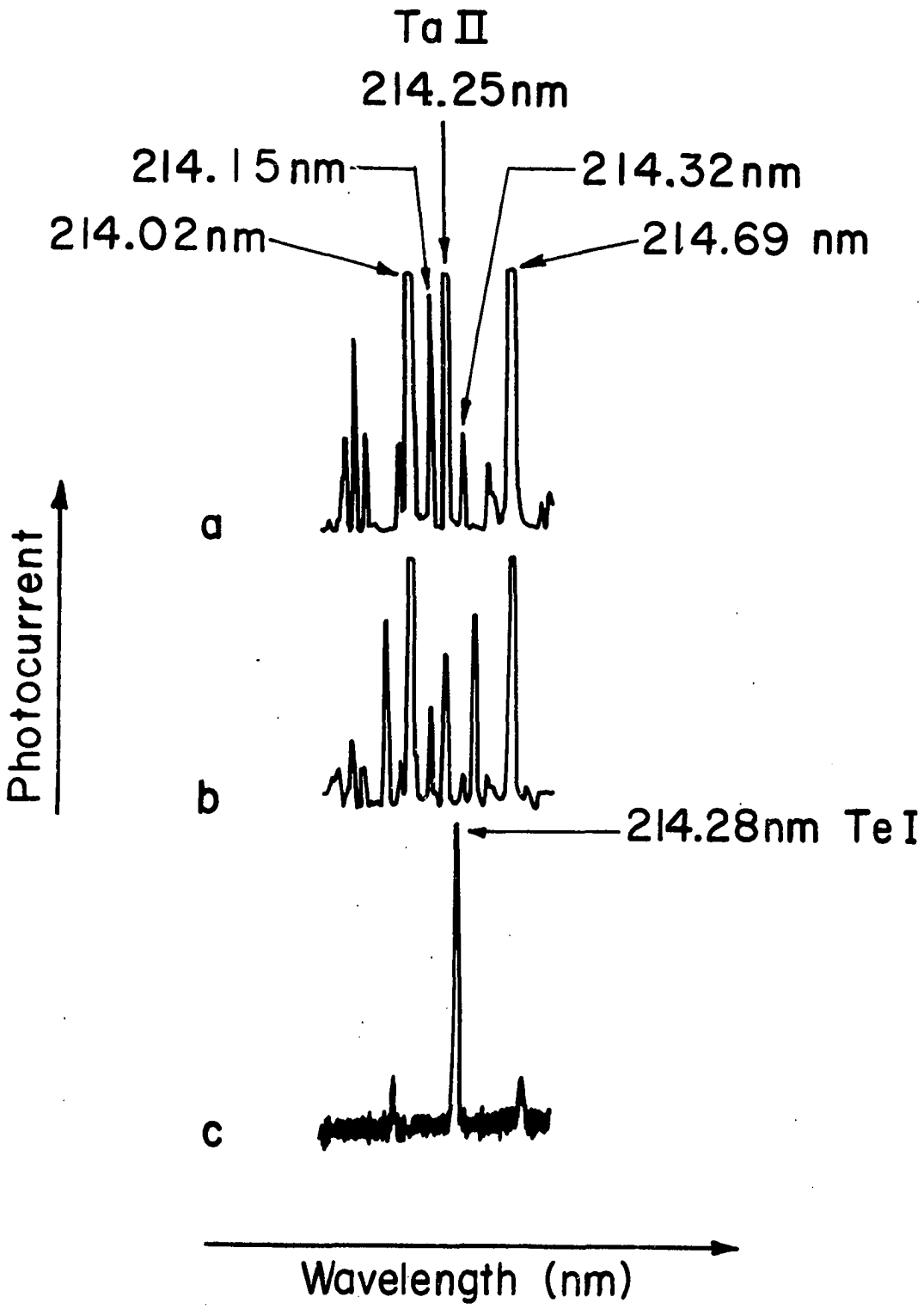
Ta II
214.25nm
214.15nm
214.32nm
214.02nm
214.69 nm
a
b
c
214.28nm Te I
Photocurrent
Wavelength (nm)

Samples introduced into the plasma:

(a) Urine from subject 1.

(b) Urine from subject 2.

(c) Urine from subject 3.

Sample introduction method:

(A) Solution nebulization

(B) Pyrolytic graphite

Vaporization temperature: (B) Approximately 2000°C; measured with an optical pyrometer.

Sample volume utilized:

(A) Continuous uptake (∿1.9 ml/min)

(B) 50 µl deposited on the filament.

Wavelength: 196.2 nm (The Se emission line is at 196.1; thus the background emission adjacent to the Se line was observed.)

Background signals resulting from these urine samples introduced into the plasma by solution nebulization (SN) and by electrothermal vaporization (EV) are shown in Figure 13. Deionized water was also introduced by both techniques to provide appropriate reference blank signals. These are also shown in the figure. The SN background signals (part A, Figure 13) contained a relatively large, high frequency noise component which resulted from the high signal amplification required for the observation of Se emission at concentrations typically found in urine. The

Figure 13. Comparison of the relative signal intensities for solution nebulization (A) and pyrolytic graphite filament vaporization (B) of three typical urine samples into the plasma

Net intensities for the solution nebulization-plasma signals are measured relative to the H_2O reference blank signal. Filament vaporization-ICP signals are measured from the Plasma Background before the pulse to the peak height

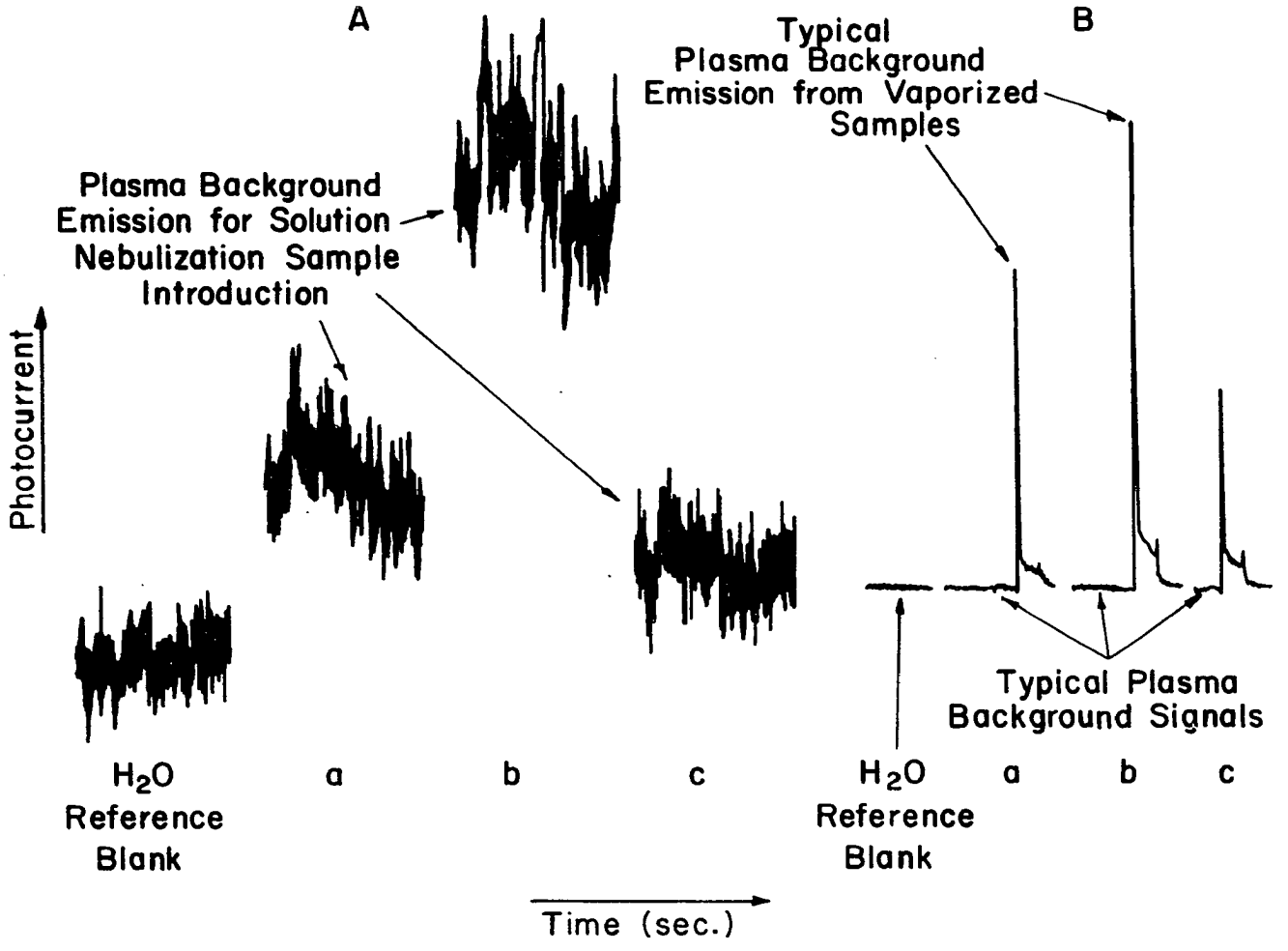
A
B
Typical
Plasma Background
Emission from Vaporized
Samples
Plasma Background
Emission for Solution
Nebulization Sample
Introduction
Photocurrent
Typical Plasma
Background Signals
H2O
Reference
Blank
a
b
c
H2O
Reference
Blank
a
b
c
Time (sec.)

important characteristics of the signals are the average values of the high frequency noise and the ratio of the average background signal levels relative to the deionized water reference blank.

As the figure shows, the urine samples produced higher background signals than the deionized water reference blank and each urine sample produced a different background signal level, whether sample introduction was by SN or by EV. Furthermore, the relative background signals (b>a>c) were in approximately the same ratio for the two sample introduction techniques. This indicates that the concomitants causing the background signals occur at varying concentrations in urine.

To determine whether any of the major constituents of urine (Na, Ca, urea) produced measurable background signals at a wavelength near the SeI 196.1 nm line, the experiments outlined below were conducted.

Part A (Figure 14)

Solutions nebulized:

(a) H_2O reference blank.

(b) 460 µg Na/ml as a solution of NaCl.

(c) 4600 µg Na/ml as a solution of NaCl.

(d) 250 µg Ca/ml as a solution of $CaCO_3$ in 5% (v/v) HCl.

(e) 1000 µg Ca/ml as a solution of $CaCO_3$ in 5% (v/v) HCl.

(f) 7.0 mg urea/ml.

(g) 50.0 mg urea/ml.

Analytical wavelength: 196.2 nm.

Part B (Figure 15)

Substrate: Pyrolytic graphite

Solutions deposited on the filament:

(a) 50 µl of an H_2O reference blank.

(b) 23.0 µg of Na in 50 µl as a solution of NaCl.

(c) 230.0 µg of Na in 50 µl as a solution of NaCl.

(d) 12.5 µg of Ca in 50 µl as a solution of $CaCO_3$ in 5% (v/v) HCl.

(e) 50.0 µg of Ca in 50 µl as a solution of $CaCO_3$ in 5% (v/v) HCl.

(f) 350 µg of urea in 50 µl.

(g) 2500 µg of urea in 50 µl.

Drying temperature: Slightly less than 100°C to avoid boiling the solution.

Vaporization temperature: 2000°C; measured with an optical pyrometer.

Analytical wavelength: 196.2 nm

In Part A (Figure 14) only (d), (e), (f), and (g) produced photocurrents greater than that of the H_2O reference blank (a). In contrast, all of the vaporized samples in Part B

(Figure 15) produced measurable intensities except the H_2O reference blank (a). In both Part A (Figure 14) and Part B (Figure 15), the presence of calcium produced the largest background signals. Insertion of a borosilicate glass filter to exclude wavelengths less than 250.0 nm from the spectrometer had no appreciable effect on the background observed for (d) and (e) in Part A or (b), (c), (d), and (e) in Part B. Thus, these signals arose from stray light contributions from the Na and Ca concomitant emissions at distant wavelengths. A more complete study of stray light effects due to inorganic concomitants has recently been submitted for publication by Larson, et al. (98).

The background contribution produced by urea (recordings (f) and (g) in Figures 14 and 15) disappeared when the borosilicate glass filter was inserted, indicating that these signals were the results of emission at wavelengths closer to the analytical lines and not due to stray light. Identification of the species that contribute to the background signals observed near the Se 196.1 nm line, as well as other analyte wavelengths, was accomplished by comparing wavelength scans of the 185 to 300 nm region while continuously nebulizing an aqueous solution containing 50 mg urea/ml with known molecular band and atomic spectra (105). The following spectra were identified:

(a) carbon atomic emission lines at 193.0 nm and 247.9 nm;

Figure 14. Solution nebulization-ICP-AES signals recorded at 196.2 nm for the following solutions: (a) deionized water; (b) 460 µg Na/ml; (c) 4600 µg Na/ml; (d) 250 µg Ca/ml; (e) 1000 µg Ca/ml; (f) 7.0 mg urea/ml; (g) 50.0 mg urea/ml


Photocurrent
a
b
c
d
e
f
g
a
Time (sec.)

Figure 15. EV-ICP-AES signals recorded at 196.2 nm with pyrolytic graphite as the vaporization substrate. The 50 µl deposited samples were: (a) a deionized water reference blank; (b) 23 µg of Na as a solution of NaCl; (c) 230 µg of Na as a solution of NaCl; (d) 12.5 µg of Ca as a solution of $CaCO_3$ in 5% (v/v) HCl; (e) 50 µg of Ca as a solution of $CaCO_3$ in 5% (v/v) HCl; (f) 350 µg of urea in deionized water; (g) 2500 µg of urea in deionized water

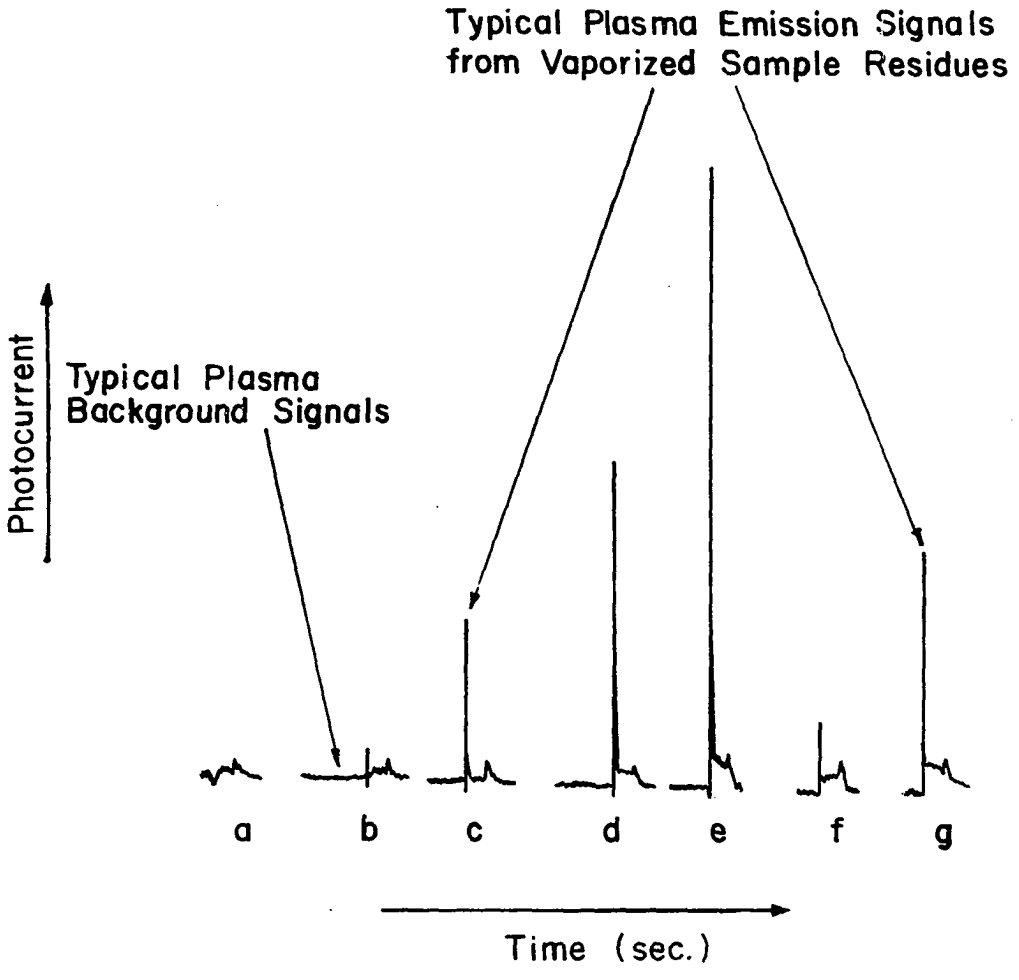
Typical Plasma Emission Signals
from Vaporized Sample Residues
Photocurrent
Typical Plasma
Background Signals
a
b
c
d
e
f
g
Time (sec.)

(b) CO and O_2 molecular band emission associated with each wavelength in (a); and

(c) NO gamma molecular band emission in a periodic progression starting around 190.0 nm and going beyond 250.0 nm.

Although these emissions normally appear in the plasma spectra at a relatively constant intensity when deionized water is nebulized, the addition of urea to the water enhances the above spectra.

Thus, the interference problem was found to arise not only from stray light produced by long wavelength inorganic emissions, but from molecular band systems enhanced by the addition of organic concomitants to the plasma. Furthermore, the magnitude of these interferences was shown to be dependent on the concentrations of several concomitants which may vary over wide concentration ranges from one biomedical sample to another.

Therefore, the determination of the subject elements at their natural concentrations in biomedical samples would be difficult at best unless means are found to reduce or compensate for these interferences.

G. Conclusion

In summary, although the EV-ICP-AES approach provided excellent powers of detection, the interelement interferences arising from physical effects or refractory compound formation

and the spectral interferences discussed in this section of the dissertation present formidable problems.

A number of experimental approaches have been conceived to reduce or possibly correct for these effects, but these schemes were considered, because of their complexity, to be unattractive for further study at this time. Attention was therefore directed towards the evaluation of procedures for separating and preconcentrating the analytes of interest from the sample concomitants prior to the analysis step.

V. PHYSIOCHEMICAL METHODS OF SEPARATION AND PRECONCENTRATION

A. Introduction

The experiments summarized in the previous section provided clear evidence that changes in the concentrations of concomitants caused such serious physical and spectral interferences in the EV-ICP-AES technique to make this approach unattractive. One obvious solution is to separate the analytes of interest from concomitants by physical and/or chemical means (physiochemical). An additional benefit would be the possibility of effecting a preconcentration of the analytes, resulting in improved powers of detection.

An ideal physiochemical separation scheme should:

1. be highly selective for the analytes of interest,
2. effect quantitative separation of the analytes from concomitants,
3. afford the capability of concentrating the analytes in biological samples by a factor of at least 100,
4. be applicable to all types of biological, biomedical, and environmental samples following digestion or dissolution,
5. permit the introduction of the resulting concentrated samples into the plasma by conventional means,

6. allow the preparation of reference standards containing the analytes in the same matrix as the unknown, and
7. be simple to execute and require inexpensive equipment.

Of the many physiochemical separation schemes that have been described and reviewed (106-110), ion exchange chromatography, liquid-liquid extraction, gaseous hydride formation, and distillation appeared to offer the greatest promise of fulfilling the criteria outlined above. A survey of the basic principles and the experimental evaluation of these methods with respect to the requirements previously listed follows. Preliminary experimental evaluation of each separation scheme was performed with the single channel facility described in Chapter 2.

B. Ion Exchange Chromatography

1. Basic principles

A stationary bed of ion exchange resin is often used to sorb ions from a liquid stream. Various types of anion and cation exchange resins have been used to sorb either analytes of concomitants by using the appropriate experimental conditions.

Cation exchange methods can be used to sorb calcium, magnesium, and other cations, while the remaining concomitants

such as organic materials and anions pass through the column. In addition, no preconcentration of the analytes of interest can be attained because they are not sorbed. Therefore, cation exchange chromatography will not be considered further.

Theoretically, anion exchange chromatography can be used to sorb anions or anionic complexes while allowing the concomitants to pass through the column. The sorbed anions are then eluted from the resin into a small volume for subsequent analysis. Typically, oxyanions such as $SeO_3^=$ and $SeO_4^=$ are sorbed onto an anion exchange resin from a slightly acidic or neutral solution (111-119). The oxyanions are then eluted with a solution which is several molar in a strong acid (e.g., HCl).

2. Experimental evaluation

Preliminary experiments on the sorption of selenium from a deionized water solution on a strong base anion exchange resin (IRA-400) in either the nitrate or chloride form produced excellent results. Selenium at concentrations ranging from 0.1 µg/ml to 1.0 µg/ml in 500 ml volumnes was sorbed onto a stationary resin bed measuring 1 cm x 5 cm. The selenium was sorbed from neutral solutions and eluted from the resin into five milliliter volumetric flasks with 4.8 molar hydrochloric acid.

Subsequent comparison of the plasma emission signals produced by the column eluates with those produced by solutions

containing known amounts of selenium in the eluant solution showed that complete recovery of selenium was achieved. Furthermore, the resulting analytical curves retained linearity previously observed for selenium in deionized water.

An attempt to sorb selenium, added to a urine sample, using the procedure described above was not successful. Twenty milliliters of this spiked urine sample was digested to near dryness with twenty milliliters of concentrated nitric acid. The residue was treated with five milliliters of a 30% hydrogen peroxide solution and again the volume was reduced. The digestion step was employed in an attempt to destroy any selenium organic complex molecules before sorption onto the resin. The resulting solution was adjusted to pH = 7 by the addition of concentrated ammonium hydroxide, and finally was introduced to the resin bed. The selenium in this solution was not sorbed on the resin. Apparently, the high nitrate concentration resulting from the nitric acid/hydrogen peroxide digestion step prevented the sorption of selenium. This is a reasonable explanation because selenium has a low distribution coefficient and is not strongly retained on an anion exchange column (111).

It was therefore concluded that the ion exchange scheme did not appear promising for the separation and preconcentration of selenium from biological samples.

C. Liquid-Liquid Extraction

1. Basic principles

Analytes can be separated from concomitants by extracting their organic chelates from an aqueous phase with an immiscible solvent. The pH, chelating agent, and extracting solvent can be varied to change the selectivity of the extraction. The method most publicized for the extraction of Group IVA, VA, and VIA elements involves the use of ammonium pyrrolidine dithiocarbamate (APDC) for the chelation followed by the extraction with methyl isobutyl ketone (MIBK) (107,109,120, 121).

2. Experimental evaluation

The APDC-MIBK extraction method, using the recommended pH values for chelate formation and extraction (121), was tested by extracting 100 micrograms of selenium into a total of 10 milliliters of MIBK. One milliliter of an aqueous solution containing 1% (w/v) APDC was used for the chelation followed by the extraction with 2 aliquots of MIBK.

A comparison of the signals observed for the plasma excitation of an aqueous selenium standard and a deionized water reference blank with the APDC-MIBK extract and reference blank showed that only a small fraction of the selenium was extracted. The incomplete extraction of selenium observed here is consistent with recently published results on the

failure of this procedure to quantitatively extract other analytes (122). The above experimental results effectively cancel any potential advantage that the extraction method could provide.

D. Hydride Formation

1. Basic principles

The formation of the gaseous covalent hydrides of As, Se, Sb, Ge, Sn and Te is accomplished by the stepwise reduction of these analytes to their lowest oxidation state followed by their combination with nascent hydrogen. Many methods have been published using a number of reducing agents (123-125); however, excellent results have been reported for the determination of arsenic and selenium in several National Bureau of Standards (NBS)-Standard Reference Materials (SRM) when sodium borohydride was used as the reducing agent and nascent hydrogen generator (126). In the past this pre-separation scheme has been extensively combined with AAS for the determination of these analytes.

2. Experimental evaluation

A method similar to the one described above was evaluated with respect to the requirements previously stated.[1] An

---

[1] S. S. Sloat, D. E. Nixon, and V. A. Fassel, Ames Laboratory USERDA, unpublished data.

aqueous solution containing 2% (w/v) sodium borohydride was introduced continuously into a 2.5 molar sulfuric acid solution containing 5 micrograms of arsenic. The arsenic plus nascent hydrogen was swept from the reaction vessel into the plasma with argon-5% hydrogen at a flowrate of 1.6 ℓ/min. This carrier gas was chosen so that the plasma tuning conditions remained reasonably constant as the gaseous reaction products passed through the plasma.

The hydride method did not produce promising results with the plasma. Even though the argon-5% hydrogen mixture was used as the aerosol carrier-gas, the nascent hydrogen plus arsenic was not easily introduced into the plasma. The rapid evolution of hydrogen, due to the fast introduction of sodium borohydride into the reaction vessel, caused the plasma to constrict and to be extinguished. A higher carrier-gas flowrate prevented this instability, but resulted in reduced analyte residence time in the high temperature region of the plasma and a consequent decrease in the analytical signal intensity.

Signals produced at the arsenic 193.7 nm wavelength were not easily interpreted. A typical recorder tracing, shown in Figure 16, depicts the photocurrent produced at the arsenic wavelength with time as the sodium borohydride was added to the acidified sample containing arsenic. The overall signal pulse returned to the original plasma background signal

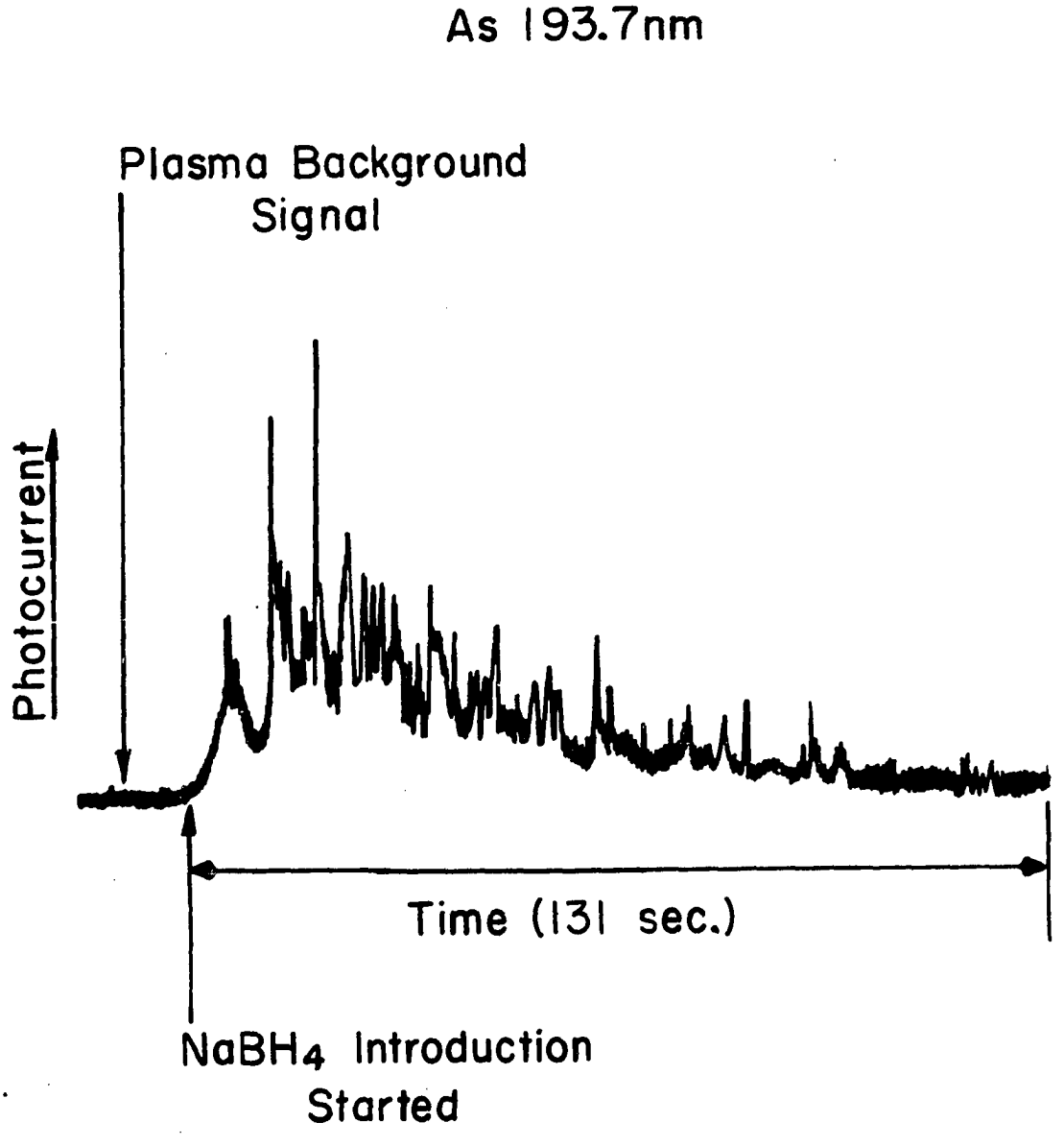

Figure 16. Emission signal produced by the plasma excitation of arsine plus nascent hydrogen

level 131 seconds after it first appeared. This slow return to the original background signal level and the individual signal pulses corresponding to the sodium borohydride solution introduction into the reaction vessel are especially noteworthy.

It was concluded that this method in its present form is not compatible with the ICP system. It was not considered further because:

1. the equipment needed to integrate the signals would be expensive; and
2. modification of the method to make it more compatible with the ICP system would require extensive research and perhaps quite different plasma conditions than those normally used.

E. Distillation

1. Basic principles

More than three quarters of a century ago selenium was separated from tellurium by the distillation of $SeBr_4$ from a mixed acid system containing KBr (127). In the interim more than 50 papers and reviews have described the distillation separation of volatile halides of Group IVA, VA, and VIA elements from concomitants. Several comprehensive studies have outlined the actual parameters for the quantitative distillation of these inorganic halide compounds

(128-133). Common procedures usually suggest the use of perchloric or sulfuric acids as the high boiling medium from which the halides are distilled after the addition of an excess of concentrated hydrobromic or hydrochloric acids. The inorganic halides, excess hydrohalic acid, and a portion of the high boiling acid are collected for subsequent analysis.

2. Experimental evaluation

a. Preliminary evaluation The procedure tested was based on a method developed by Hoffman and Lundell (128). Their results indicated that more Group IVA, VA, and VIA elements are quantitatively distilled from the combination of perchloric acid with hydrobromic than from other mixtures.

Initially, the separation scheme was tested by adding three milliliters of concentrated hydrobromic acid to a Kjeldahl digestion flask containing 25 micrograms of As, Se, Sn, Ge, Te, Sb, and Hg in 10 milliliters of concentrated perchloric acid. The apparatus shown in Figure 17 was used for the distillation. The Kjeldahl flask, modified by adding the standard taper ground glass joint, and the distillation head were constructed from borosilicate glass. A heating mantle was placed snugly beneath the Kjeldahl flask.

With argon flowing through the flask, bubbling through the delivery tip and into 1.5 milliliters of water in the five milliliter volumetric receiver, the rheostat was

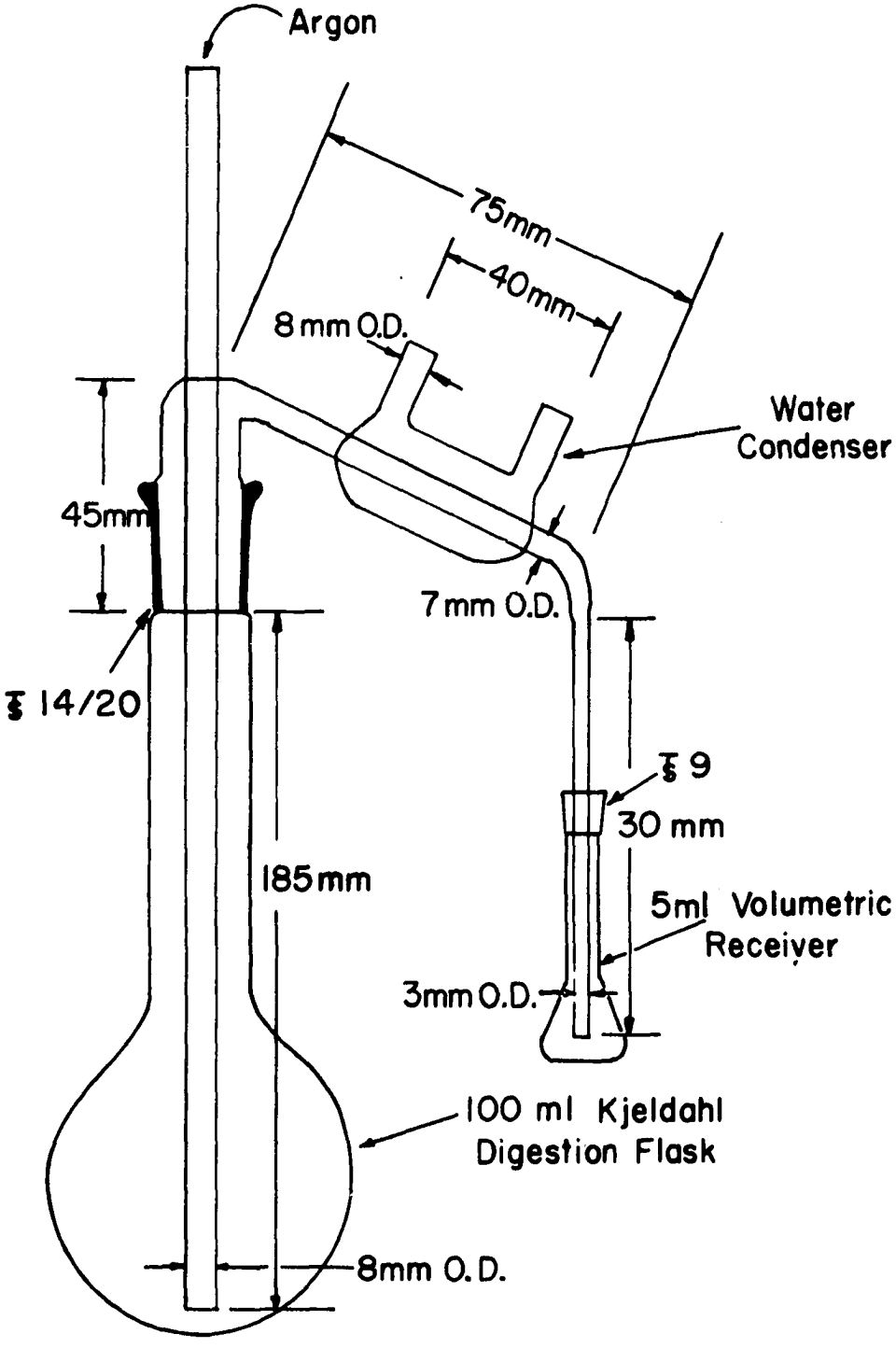

Figure 17. The distillation apparatus

adjusted to deliver 90% of the line voltage to the 230 W heating mantle. The transfer of distillate vapors, aided by argon bubbling through the system at a rate sufficient to prevent the liquid in the receiver from backing up into the tip, continued until fumes of perchloric acid appeared in the Kjeldahl flask (approximately 215°C). The separation was completed by the distillation of 0.5 milliliters of perchloric acid to remove residual hydrobromic acid from the distillation head and fill the volumetric receiver to the 5 milliliter mark.

b. Results The ICP-SMEA signals produced by the distillate and a reference standard prepared by mixing the analytes, H_2O, HBr, and $HClO_4$ in the quantities assumed to be present in the distillate were compared. The background or reference blank signal was established by nebulizing a solution containing all of the above components except the analytes. Only partial distillation of Sb and Hg was obtained and essentially no distillation of Te was observed. A comparison of the signals produced by the subsequent aspiration of the reference standard and distillate as shown in Figure 18 revealed that quantitative transfer of As, Se, Sn, and Ge was attained.

The nebulization of a reference blank solution following the introduction of a reference standard solution usually returns the analytical signal to the original reference

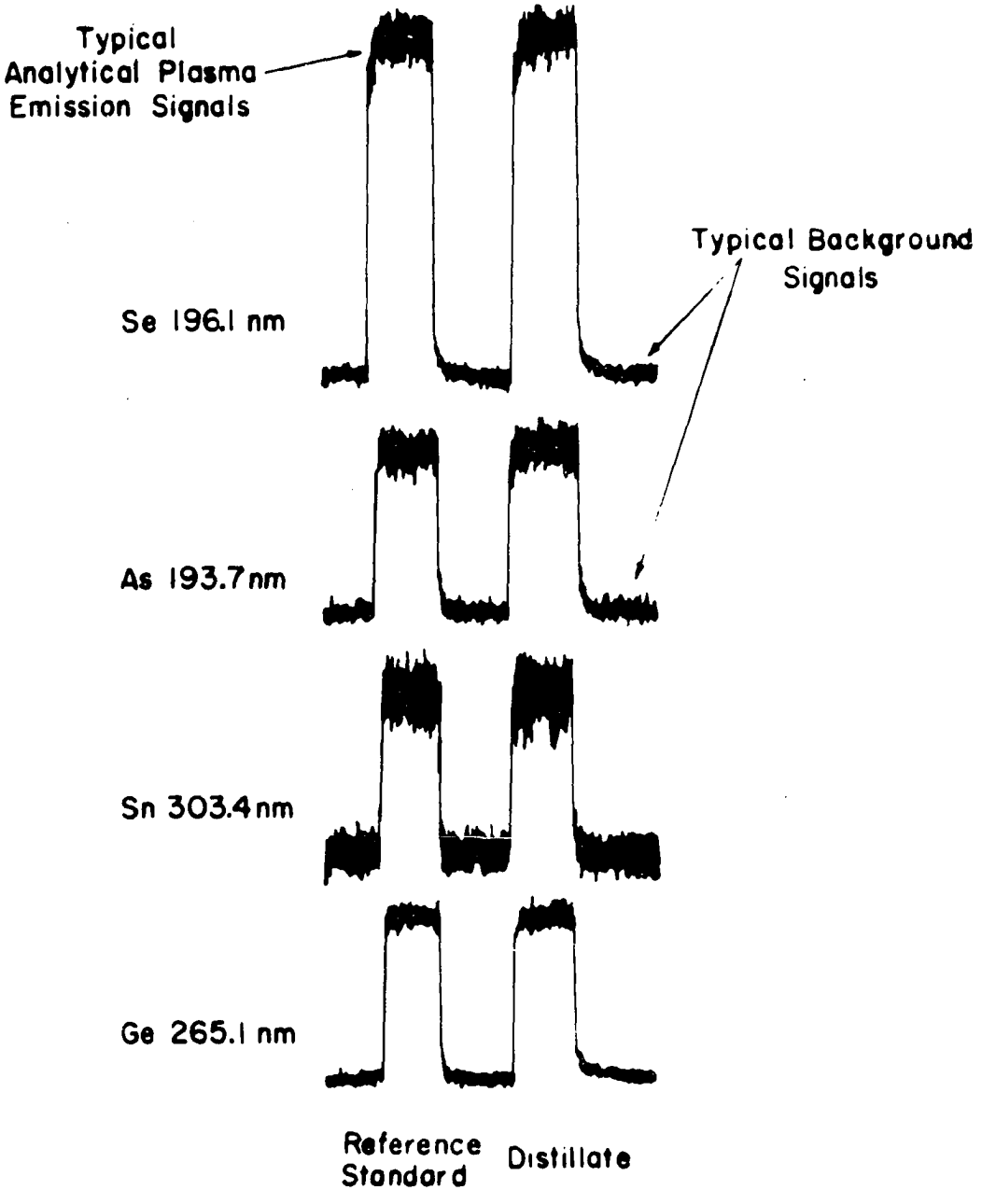

Figure 18. Typical reference standard and distillate plasma emission signals for Se, As, Sn, and Ge, each at a concentration of 5 µg/ml

blank level. However, the signal produced by the reference blank nebulized after a reference standard, containing volatile elements in a hydrohalic acid medium, may require several minutes to return to its original level. This "memory effect" or spray chamber "clean out" phenomenon has been described for As, Se, and other volatile elements (134,135). The distillation of three milliliters of concentrated HBr and 0.5 milliliters of $HClO_4$ into a five milliliter volumetric flask was found to be the maximum acceptible acid concentration. Higher concentrations of HBr or $HClO_4$ produced analyte signals that slowly returned to the reference blank signal level. At these high acid concentrations the Se signals produced a pronounced "memory effect", but As, Ge, and Sn signals did not. In this study no "memory effect" was encountered when the distillation procedure outlined above was followed.

A comparison of the simultaneous multielement detection limits observed for the elements prepared in aqueous and $HBr/HClO_4$ solutions without distillation is shown in Table VI. The detection limits, observed under comparable conditions for both matrices, are essentially identical.

The analytical curves shown in Figure 19 were obtained by plotting the net integrated signal intensities recorded for each analyte simultaneously versus the concentration of each multielement reference standard prepared in the $HBr/HClO_4$

Table VI. ICP-SMEA detection limits

Element	Wavelength (nm)	Aqueous Detection (µg/ml)	$HBr/HClO_4$ Detection Limits (µg/ml)
As	193.7	0.04	0.02
Se	196.1	0.02	0.03
Sn	303.4	0.06	0.04
Ge	265.1	0.02	0.02

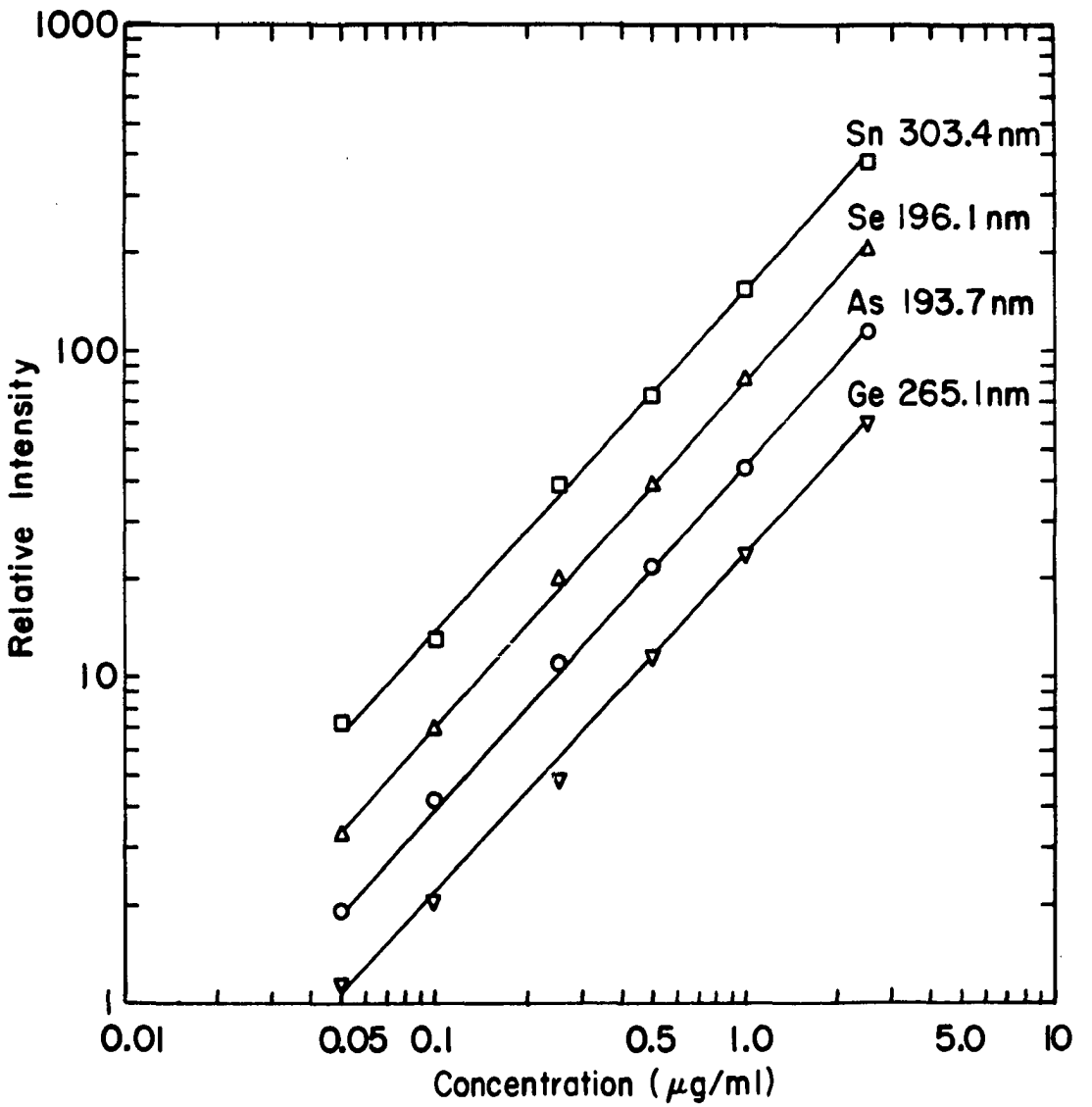

Figure 19. Analytical curves for the ICP-SMEA determination of As, Se, Sn, and Ge in an $HBr/HClO_4$ matrix

solution without distillation. It can readily be seen that under one set of analysis conditions the analytical curves are parallel and linear as they approach the detection limit concentration.

At least for one synthetic test matrix, the distillation separation technique fulfills the majority of the requirements listed previously. The applicability of this technique for the separation and preconcentration of As, Se, Sn, and Ge from biological, biomedical, and environmental samples was evaluated next.

3. Simultaneous multielement analysis of real samples

It is perhaps coincidental that perchloric acid was found both to be a convenient medium for the distillation of the volatile halides and an excellent oxidizing agent. In the latter capacity the combination of concentrated nitric and perchloric acids are conveniently used to mineralize biological and environmental samples following the classical "liquid fire" digestion procedure outlined by Smith (136) and Diehl (137). This procedure provides complete retention of the volatile elements in a perchloric acid matrix ready for the distillation of the volatile bromides as outlined above.

a. Procedure The wet oxidation of samples was performed in a stainless steel hood (The Baker Co., Biddleford, ME) with a Labconco digestion apparatus (Labconco Corp., Kansas City, MO; Catalogue No. 60300C). The digestion

apparatus consists of a borosilicate glass fume collection manifold and six coil heaters with continuously variable individual heating controls. The manifold is connected to a water trap containing a saturated sodium hydroxide solution. Suction from a water driven aspirator was used to pull the acid fumes from the manifold through the trap and finally down the drain.

Standard Reference Materials (SRM's) prepared by the National Bureau of Standards (NBS) (138) were obtained in order to verify the accuracy of the digestion-distillation scheme. The elements present in the SRM's were determined by the NBS by two independent analytical techniques and each elemental concentration is certified to be within a specified range of values.

Typically, five gram samples of Orchard Leaves (SRM 1571) and Bovine Liver (SRM 1577) or one gram of Coal (SRM 1630 and SRM 1632) were weighed into individual 100 milliliter borosilicate glass Kjeldahl flasks. Two 5 milliliter portions of concentrated nitric acid were added to each digestion flask at intervals several minutes apart. A time span of up to one hour passed before 10 milliliters of concentrated perchloric acid was added. The addition was made sooner if no or very little frothing occurred. A piece of tetrafluoroethylene bar approximately 6.4 mm x 20 mm was added to each flask to prevent bumping when heat was applied.

These prepared samples plus a reagent blank sample were allowed to predigest at room temperature for 24 hours before applying heat. The samples were then heated by slowly increasing the temperature until nitrogen dioxide evolution started. This temperature was maintained until the rate of NO_2 evolution decreased. At this point the solutions started to appear lighter in color. The temperature was then elevated to produce vigorous boiling and nitric acid reflux on the neck of the Kjeldahl flasks. The digestion was terminated when white fumes of perchloric acid appeared in the flasks. Execution of the distillation separation procedure followed for each sample after the samples had cooled to room temperature.

b. Results The accuracy (recovery) of the overall digestion-distillation scheme was tested by analyzing the NBS-SRM's described above. The separated analytes were determined simultaneously in each sample using the ICP-SMEA facility described in Chapter 2, section B. The ICP-SMEA system was calibrated with multielement reference standards and a reference blank prepared with the same quantities of HBr, H_2O, and $HClO_4$ as contained in the distillates.

Table VII compares the certified values with the values obtained by the procedure described above. Excellent agreement was obtained for all of the results with the exception of As in Bovine Liver (SRM 1577). The repeatability, as

Table VII. Analysis of Standard Reference Materials (SRM)

Material	SRM	Element	ICP-Distillation Procedure (μg/g)	NBS (μg/g)
Bovine Liver	1577	As	0.29±0.11	(0.06)[a]
		Se	0.97±0.03	1.1±0.1
		Sn	0.22±0.18	--[b]
		Ge	N.D.[c]	--
Orchard Leaves	1571	As	8.8±0.4	11±2
		Se	0.07±0.004	0.08±0.01
		Sn	0.34±0.09	--
		Ge	N.D.	--
Coal	1632	As	6.5±0.5	5.9±0.6
		Se	2.9±0.1	2.9±0.3
		Sn	4.0±0.2	--
		Ge	N.D.	--
Coal	1630	Se	2.12±0.09	(2.1)

[a]Parentheses indicate concentration values listed by the NBS as tentative.

[b]-- Not determined by the NBS.

[c]N.D. = not detected.

indicated by the ± one standard deviation values for the triplicate determinations, was also acceptable.

The precision of the total procedure (weighing, digestion, distillation, and instrumental calibration) was estimated by preparing and analyzing twelve separate "synthetic" Orchard Leaf samples. These samples were prepared as follows. Individual portions of NBS-SRM No. 1571 weighing from 3.1 to 5.0 grams were taken through the wet oxidation procedure. At this point in the procedure quantities of Se, Sn, and Ge were added so that the final concentrations after distillation consisted of 0.3 ppm of the above elements in addition to their residual concentrations. The additions were made to bring the elemental concentrations into a range suitable for quantitative measurement (approximately 10 times the detection limit). Because it was not detected initially, Ge was added to the NBS-SRM. The analytes were then distilled in the usual manner. The individual distillates were then analyzed over a period of five days, after recalibration of the polychromator-ICP system before each analysis run. Only one distillate was analyzed per recalibration.

The results in Table VIII show that excellent overall precision was observed. Repeated recalibration and analysis of individual samples produced an overall relative standard deviation of approximately 0.05 for As, Se, and Sn.

Table VIII. Precision of the analytical procedure for the analysis of "synthetic" Orchard Leaf samples

Material	SRM	Element	ICP-Distillation Procedure		NBS	
			Nominal[a] Conc.	RSD[b]	Certified[a] Conc.	RSD[b]
Orchard Leaves	1571	As	10.9±0.6	0.055	11±2	0.182
		Se	0.37±0.02	0.054	--[c]	--[c]
		Ge	0.28±0.04	0.143	--	--
		Sn	0.64±0.03	0.047	--	--

[a]All values listed are in terms of μg/g of sample.

[b]RSD is the Relative Standard Deviation.

[c]A comparison of the Certificate values with the "synthetic" values is not applicable.

The above results indicate that the "liquid fire" digestion followed by the distillation of the volatile bromides is a useful separation scheme. Furthermore, the results suggest that a wide variety of samples can be analyzed using the same calibration curves.

4. Analysis of biofluids

The digestion-distillation scheme can be directly applied for the separation of As, Se, Sn, and Ge from concomitants in biofluids. In addition, a certain amount of preconcentration can be achieved prior to the determination step. This is an important additional benefit because the elements of interest are normally present in biofluids at very low concentrations. The procedures used for collection of specimens and analytical results for the determination of As, Se, Sn, and Ge in human whole blood, blood serum, and urine are described below.

a. Sample collection and preparation

1. Urine Urine specimens were collected by healthy adult males for 24-hour periods refrigerating the polyethylene bottle after each addition. The collected specimens were then either frozen without added preservative or analyzed immediately.

2. Whole blood Human whole blood samples were obtained from male and female adults during routine medical examinations. The samples were drawn using 21 gauge stainless steel needles and polyethylene syringes. Two drops of a

15% (w/v) solution of dipotassium EDTA per 5-milliliters of blood were used to prevent clotting. The pooled samples were refrigerated until needed.

3. Serum Five healthy adult male volunteers donated 50 milliliters of whole blood each. The samples were poured into test tubes, allowed to clot, then spun down in a centrifuge. The serum was drawn off, pooled in a fluorinated ethylene-propylene copolymer (FEP) bottle, and frozen.

Frozen samples were thawed in a commercial microwave oven operated in the defrost mode and refrigerated samples were allowed to reach room temperature before aliquots were removed for analysis. Typically, 50 milliliters of urine or 25 milliliters of whole blood or serum were digested using 10 milliliters each of concentrated nitric and perchloric acids. The volatile bromides were distilled into five milliliter volumetric receivers as described above.

b. Results A comparison of the ICP-SMEA results with normal values found in the literature is shown in Table IX. Good agreement with the literature values and adequate precision for several determinations were attained.

The analytical results of the determination of As, Se, Sn, and Ge in aliquots of three different 24-hour urine samples are shown in Table X. The comparison illustrates that the digestion-distillation procedure followed by the

Table IX. Analysis of human biofluids

Biofluid	Element	ICP-Distillation Procedure (µg/ml)	Typical Reported Values (µg/ml)	Literature References
Whole Blood	As	0.016±0.006	0.001-0.92	139
	Se	0.182±0.010	0.10-0.34	140
	Sn	0.032±0.009	0.12	141
	Ge	0.006±0.003	--	--
Serum	As	0.032	0.0-0.05	142
	Se	0.162	0.05-0.15	142
	Sn	0.032	0.0-0.47	142
	Ge	N.D.[a]	0.0-0.10	142
Urine	As	0.036±0.004	0.03-0.14	143
	Se	0.050±0.005	0.01-0.15	4
	Sn	0.011±0.005	0.013-0.015	141
	Ge	N.D.	--	--

[a]N.D. = not detected.

Table X. Comparison of trace element concentrations in several 24-hour urine specimens

Element	Concentration (μg/ml)		
	Specimen 1	Specimen 2	Specimen 3
As	0.025±0.011	0.016±0.003	0.036±0.004
Se	0.036±0.005	0.027±0.002	0.050±0.005
Sn	0.031±0.006	0.028±0.007	0.011±0.005
Ge	N.D.[a]	N.D.	N.D.

[a]N.D. = not detected.

ICP-SMEA determination permits a direct comparison of elemental concentrations in a particular sample with those in other samples of the same type.

One final evaluation of the digestion-distillation scheme was performed by comparing the results of standard additions of the four analytes to urine with a reference standard analytical curve for each element. The method of standard additions can be used to determine the consistency of the analyte emission behavior in the real matrix (linear plots of relative intensity vs concentration of analyte added). If the spectral backgrounds produced by the

standard addition and calibrating samples are the same and the residual elemental intensities are subtracted from the standard addition curves, the coincidence of the two curves suggests that the nebulization and emission characteristics of the solution are identical.

The method of standard additions was implemented by adding increasing quantities of As, Se, Sn, and Ge to 50 milliliter portions of a 24-hour urine specimen. These samples were taken through the digestion and distillation steps outlined previously. The standard addition curves for the urine samples (squares) and the reference standard analytical curves (circles) are shown in Figures 20a to 20d for each element.

Because the distillates and reference standards were prepared so that they contained the same matrix constituents, the same spectral backgrounds were obtained for each sample type and a correction for the residual Se, As, Sn, and Ge concentrations in the urine specimens brought the standard addition points into coincidence with the calibration curves. These results indicate that the analytes were quantitatively retained by the digestion procedure independent of their original form and that the volatile bromides were completely distilled. Furthermore, these coincident curves indicate that the sample nebulization and emission characteristics of the distillates were the same as those of the reference standards.

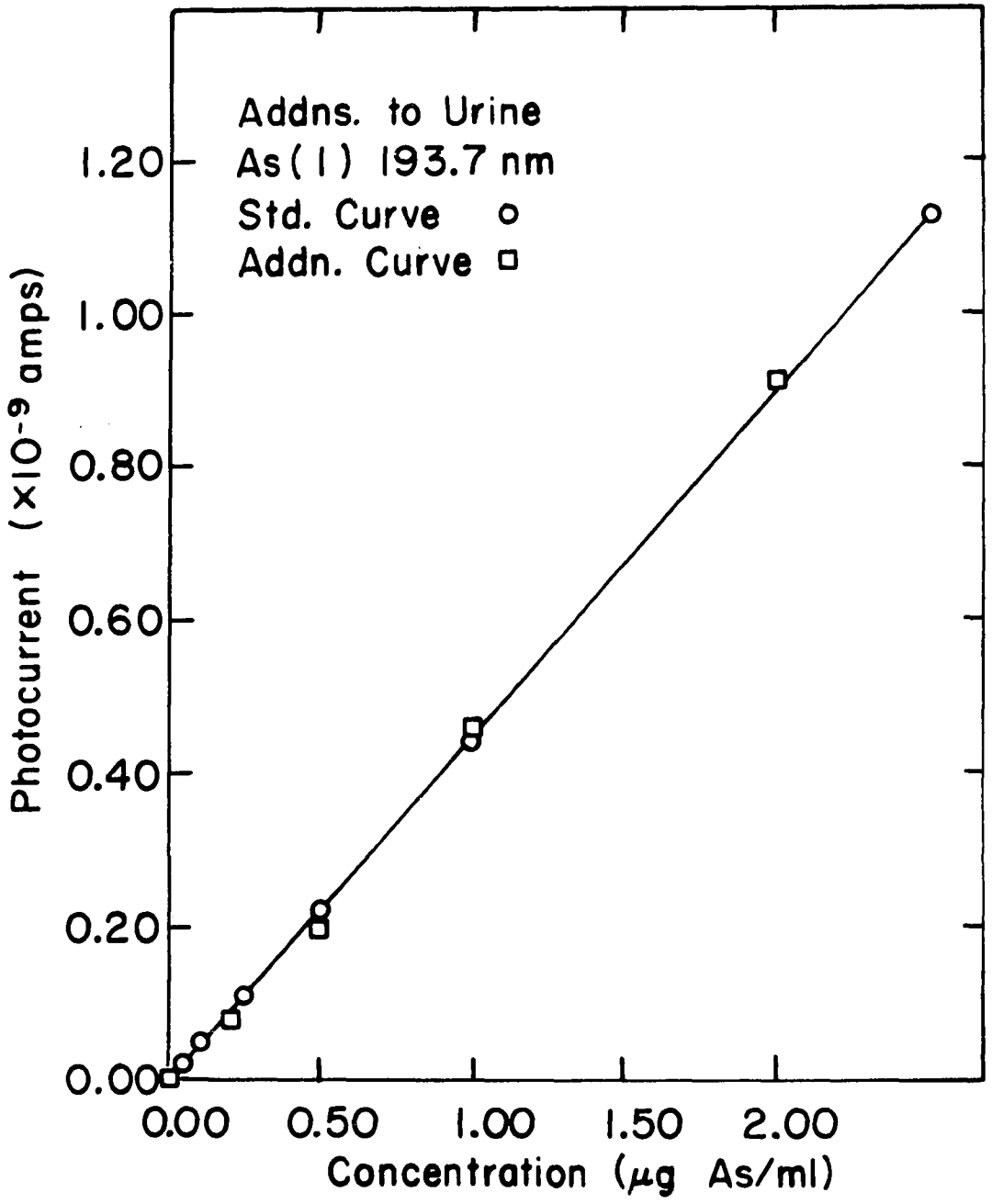

Figure 20a. Standard addition and reference standard cruves for As

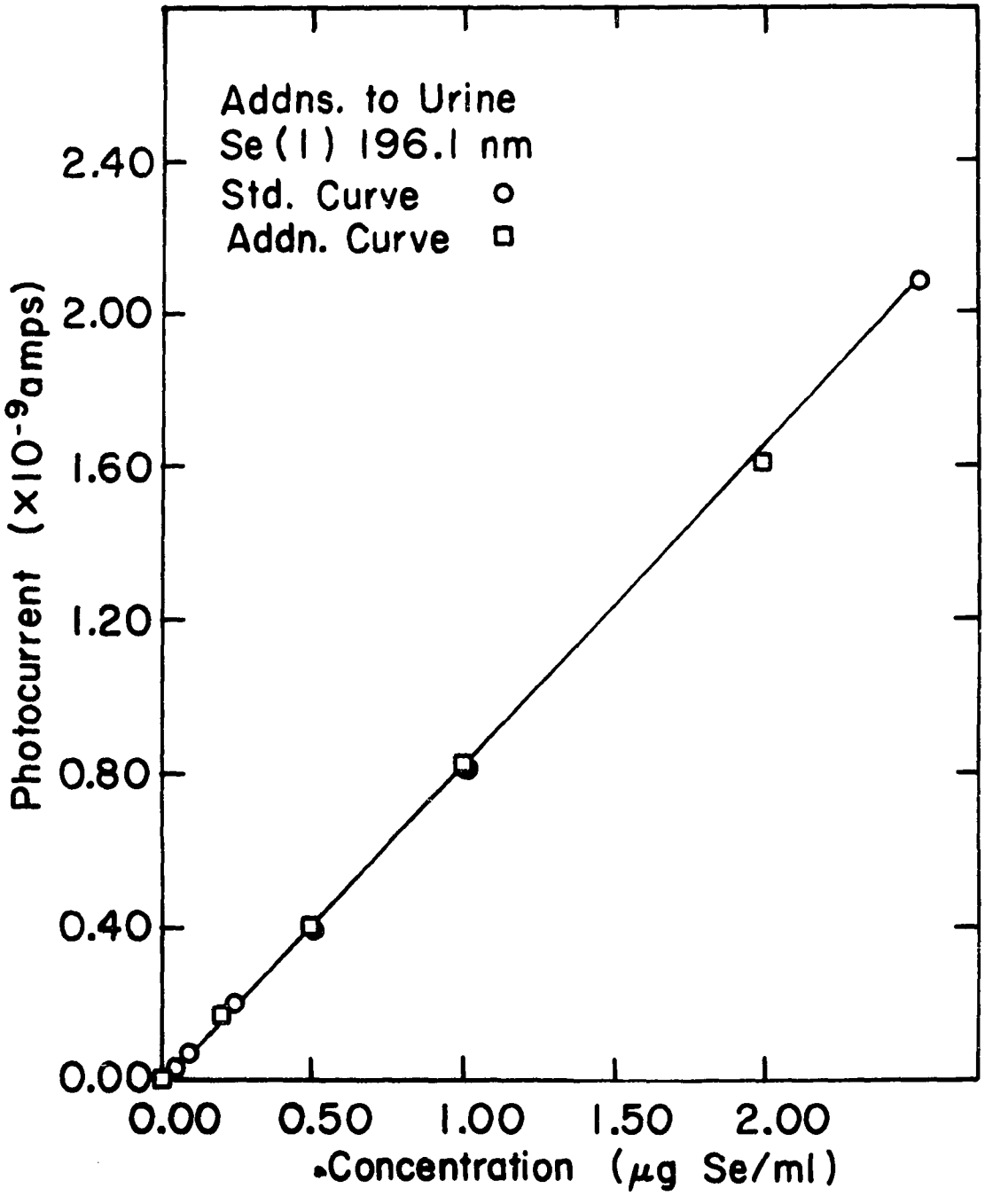

Figure 20b. Standard addition and reference standard curves for Se

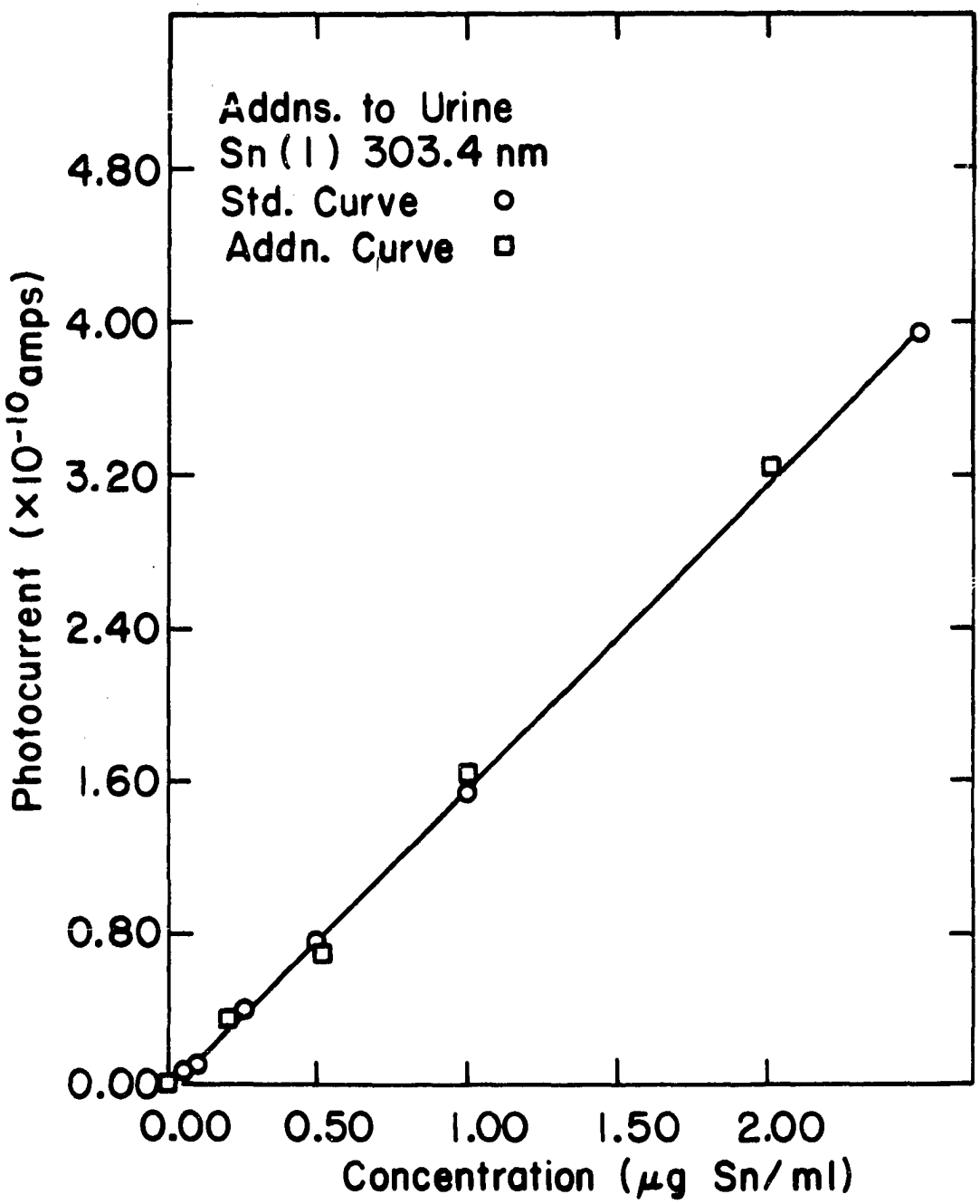

Figure 20c. Standard addition and reference standard curves for Sn

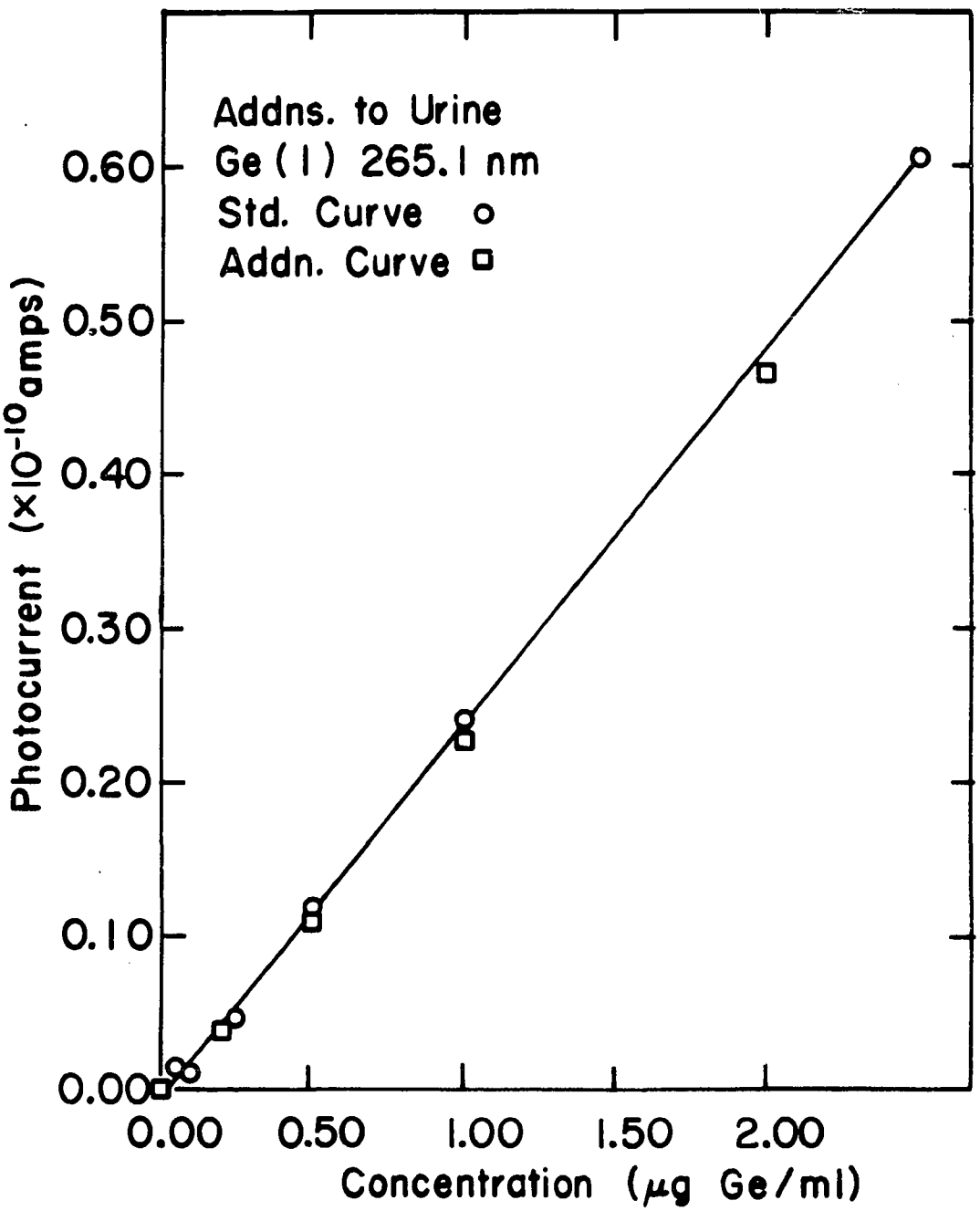

Figure 20d. Standard addition and reference standard curves for Ge

F. Conclusion

Of the four separation schemes evaluated, only the distillation method met all of the previously listed requirements of an ideal separation procedure. This simple approach provides excellent separation of the analytes from concomitants and can provide preconcentration of the elements of interest. The procedure can be performed in a reasonable amount of time and requires only minimal equipment expenditures.

VI. CONCLUSIONS

The conclusions drawn from the foregoing research can be stated simple.

1. The present pneumatic nebulization system cannot effectively introduce the quantity of analyte into the plasma needed to produce adequate powers of detection for the determination of As, Se, Te, Sb, Sn, and Ge at ultratrace concentrations.

   In addition, the presence of stray light from the emission of concomitants present in real samples seriously detracts from the otherwise attractive features of the ICP-SMEA system. This serious flaw is <u>not</u> associated with the plasma, but is due to defects in the optical components.

2. The adaptation of the much publicized thermal vaporization and atomization technique to the ICP proved to be successful only for the analysis of essentially pure water solutions containing analytes at trace concentrations. The numerous constraints and limitations discovered for the analysis of real samples effectively nullify any advantages thought to

be derived from the coupling of an EV device to the ICP.

3. Of the many physiochemical separation and preconcentration methods investigated, only the distillation method was completely compatible with the present plasma facilities. This separation scheme provided a convenient, simple, inexpensive, and highly specific method for the quantitative isolation of As, Se, Sn, and Ge from concomitants present in biomedical and environmental samples.

In addition, the determination of very low analyte concentrations in biofluids was implemented by the preconcentration provided by the digestion-distillation approach.

VII. SUGGESTIONS FOR FUTURE RESEARCH

The following investigations would be logical extensions of this dissertation research. Some of the projects outlined have already been initiated in this laboratory.

Improvements in the ICP powers of detection and elimination or compensation for the stray light spectral background interference are of highest importance.

Presently, the weakest link in the SN-ICP approach is the sample introduction device. Typical low flow pneumatic nebulizers deliver approximately 5 to 10% of the original sample to the plasma.

Near the end of this dissertation research, a paper was published which described the ultrasonic sample nebulization followed by the aerosol desolvation prior to the plasma excitation (144). This approach resulted in more than an order of magnitude improvement in the ICP detection limits as compared with pneumatic nebulization (see Table XI). Thus, work proceeding in the laboratory has focused on the development of an ultrasonic nebulization system (47).

A correction method for spectral background shifts could be made by rapidly scanning the spectral line and the adjacent background with an oscillating quartz or sapphire refractor plate mounted behind the spectrometer entrance slit (145). With the spectrometer focused on the analytical wavelength, the refractor plate, driven at a set frequency,

Table XI. Comparison of detection limits

Element	Detection Limits (µg/ml)	
	Ultrasonic Nebulization (144)	Pneumatic Nebulization
As	0.006	0.03
Sn	0.003	0.06
Ge	0.005	0.02

moves the spectral image across the exit slit a distance dependent on the angle of the plate rotation and the refractive index of the material. The signal recorded at twice the scanning frequency is the second derivation of the original signal. If no discontinuities are present in the adjacent background, these signals would be zero and the only positive signal would be the actual line intensity.

Work on the hydride generation technique should continue because this method could provide a very specific and rapid separation of the Group IVA, VA, and VIA elements.

The halide distillation technique could be further refined to produce quantitative separation of the higher boiling halide compounds of Sb, Cr, Te, and Hg.

High pressure liquid chromatography (HPLC) might be utilized for the separation of analytes from interfering concomitants. The analytes could be eluted from the HPLC column directly to the nebulizer of the ICP-SMEA system.

VIII. BIBLIOGRAPHY

1. L. Ember, Environ. Sci. Technol. 9, 1116 (1975).

2. W. H. Allaway, in Trace Analysis, Physical Methods, edited by G. H. Morrison (Interscience, New York, 1965), Chapter 3, p. 67.

3. T. W. Clarkson and V. Di Stefano, in Drill's Pharmacology in Medicine, 4th ed., edited by J. R. DiPalma, M.D. (McGraw-Hill, New York, 1971), Chapter 53, p. 1101.

4. H. C. Hodge, L. J. Leach, F. A. Smith, W. H. Strain, and D. R. Taves, in Drill's Pharmacology in Medicine, 4th ed., edited by J. R. DiPalma, M.D. (McGraw-Hill, New York, 1971), Chapter 54, pp. 1120, 1131.

5. D. H. Klein, A. W. Andren, J. A. Carter, J. F. Emery, C. Feldman, W. Fulkerson, W. S. Lyon, J. C. Ogle, Y. Talmi, R. I. Van Hook, and N. Bolton, Environ. Sci. Technol. 9, 973 (1975).

6. Chem. Eng. News, Jan. 26, 1976, p. 7.

7. W. L. Zemaitis, in Environmental Health, edited by P. W. Purdom (Academic Press, New York, 1971), Chapter 4, p. 154.

8. Water Quality Criteria, Report of the National Technical Advisory Committee to the Secretary of the Interior, Federal Water Pollution Control Administration (U. S. GPO, Washington, D.C., 1968), p. 20.

9. Chem. Eng. News, Jan. 19, 1976, p. 20.

10. Environ. Sci. Technol. 10, 215 (1976).

11. E. J. Underwood, Trace Elements in Human and Animal Nutrition, 3rd ed. (Academic Press, New York, 1971), pp. 11, 323, 427, 436, 450.

12. J. G. Reinhold, Clin. Chem. 21, 476 (1975).

13. H. J. M. Bowen, Trace Elements in Biochemistry (Academic Press, London, 1966), Chapter 5, p. 81; Chapter 7, p. 102; Chapter 11, p. 159.

14. M. R. Spivey Fox, in Metallic Contaminants and Human Health, edited by D. H. K. Lee (Academic Press, New York, 1972), Chapter 8, p. 192.

15. K. Schwarz, in Newer Trace Elements in Nutrition, edited by W. Mertz and W. E. Cornatzer (Marcel Dekker, New York, 1971), Chapter 13, p. 313.

16. R. A. Zingaro and W. C. Cooper, eds., Selenium, (Van Nostrand Reinhold, New York, 1974).

17. I. Rosenfeld and D. A. Beath, Selenium (Academic Press, New York, 1964).

18. W. A. Krehl, Nutrition Today 5, 26 (1970).

19. E. Frieden, Scientific American 227, 52 (1972).

20. R. J. Shamberger, S. A. Tytko, and C. E. Willis, in Proceedings of the Trace Substances in Environmental Health - IX, edited by D. D. Hemphill (University of Missouri Press, Columbia, MO., 1975), p. 15.

21. D. V. Frost, Chem. Eng. News, Dec. 1, 1975, p. 3.

22. F. H. Nielsen and H. H. Sandstead, Amer. J. Clin. Nutr. 27, 515 (1974).

23. O. E. Olson, I. S. Palmer, and E. I. Whitehead, in Methods of Biochemical Analysis, edited by D. Glick (John Wiley and Sons, New York, 1973), Vol. 21, p. 39.

24. L. B. Tepper, in Metallic Contaminants and Human Health, edited by D. H. K. Lee (Academic Press, New York, 1972), Chapter 10, p. 229.

25. W. C. Cooper, in Selenium, edited by R. A. Zingaro and W. C. Cooper (Van Nostrand Reinhold, New York, 1974), Chapter 10, p. 646.

26. V. A. Fassel and R. N. Kniseley, Anal. Chem. 46, 1110A (1974).

27. R. N. Kniseley, V. A. Fassel, and C. C. Butler, Clin. Chem. 19, 807 (1973).

28. R. H. Scott, V. A. Fassel, R. N. Kniseley, and D. E. Nixon, Anal. Chem. 46, 75 (1974).

29. S. Greenfield, I. Ll. Jones, H. McD. McGeachin, and P. B. Smith, Anal. Chim. Acta 74, 225 (1975).

30. V. A. Fassel and R. N. Kniseley, Anal. Chem. 46, 1155A (1974).

31. S. Greenfield, I. L. Jones, and C. T. Berry, Analyst 89, 713 (1964).

32. S. Greenfield, Proc. Soc. Anal. Chem. 2, 111 (1965).

33. S. Greenfield, P. B. Smith, A. E. Breeze, and N. M. D. Chilton, Anal. Chim. Acta 41, 385 (1968).

34. R. H. Wendt and V. A. Fassel, Anal. Chem. 37, 920 (1965).

35. R. H. Wendt and V. A. Fassel, Anal. Chem. 38, 337 (1966).

36. W. Barnett and V. A. Fassel, Spectrochim. Acta 23B, 643 (1968).

37. V. A. Fassel and G. W. Dickinson, Anal. Chem. 40, 247 (1968).

38. G. W. Dickinson and V. A. Fassel, Anal. Chem. 41, 1021 (1969).

39. V. A. Fassel, ASTM Spec. Tech. Pub., (in press).

40. D. J. Kalnicky, R. N. Kniseley, and V. A. Fassel, Spectrochim. Acta 30B, 511 (1975).

41. H. R. Sobel, R. N. Kniseley, W. L. Sutherland, and V. A. Fassel, paper No. 339, presented at the 1975 Pittsburgh Conference on Analytical Chemistry and Applied Spectroscopy, Cleveland, OH., March 3-7, 1975.

42. R. H. Scott and A. Strasheim, Anal. Chim. Acta 76, 71 (1975).

43. R. K. Winge, V. A. Fassel, W. Sutherland, and R. N. Kniseley, to be submitted to Anal. Chem. for publication.

44. G. F. Larson, V. A. Fassel, R. H. Scott, and R. N. Kniseley, Anal. Chem. 47, 238 (1975).

45. R. N. Kniseley, H. Amenson, C. C. Butler, and V. A. Fassel, Appl. Spectrosc. 28, 285 (1974).

46. V. A. Fassel, in the XVI Colloquium Spectroscopicum Internationale, Heidelberg, 1971 (Adam Hilger, London, 1972), p. 63.

47. K. W. Olson, W. J. Haas, Jr., and V. A. Fassel, to be submitted to Anal. Chem.

48. G. F. Kirkbright, A. F. Ward, and T. S. West, Anal. Chim. Acta 62, 241 (1972).

49. G. F. Kirkbright, A. F. Ward, and T. S. West, Anal. Chim. Acta 64, 353 (1973).

50. C. C. Wohlers, Iowa State University, (unpublished data).

51. B. V. L'vov, Spectrochim. Acta 17, 761 (1961).

52. H. Massmann, Spectrochim. Acta 23B, 215 (1968).

53. F. Woodriff, R. W. Stone, and A. M. Held, Appl. Spectrosc. 22, 408 (1968).

54. B. V. L'vov, Spectrochim. Acta 24B, 53 (1969).

55. B. V. L'vov, Pure and Appl. Chem. 23, 11 (1970).

56. D. C. Manning, and F. Fernandez, Atomic Absorption Newsletter 9, 65 (1970).

57. R. W. Marrow and R. J. McElhaney, presented at the Sixteenth Conference on Analytical Chemistry in Nuclear Technology, Gatlinburg, Tennessee, 1972.

58. F. J. Fernandez and D. C. Manning, Atomic Absorption Newsletter 10, 65 (1971).

59. H. L. Kahn, Amer. Lab., August 1971, p. 35.

60. G. P. Sighinolfi, Atomic Absorption Newsletter 11, 96 (1972).

61. G. Baudin, M. Chaput, and L. Feve, Spectrochim. Acta 26B, 425 (1971).

62. T. S. West and X. K. Williams, Anal. Chim. Acta 45, 27 (1969).

63. R. G. Anderson, I. S. Maines, and T. S. West, Anal. Chim. Acta 51, 355 (1970).

64. M. D. Amos, P. A. Bennett, K. G. Brodie, P. W. Y. Lung, and J. P. Matousek, Anal. Chem. 43, 211 (1971).

65. J. P. Matousek, Amer. Lab., June 1971, p. 45.

66. J. Aggett and T. S. West, Anal. Chim. Acta 55, 349 (1971).

67. D. Alger, R. G. Anderson, I. S. Maines, and T. S. West, Anal. Chem. Acta 57, 271 (1971).

68. R. G. Anderson, H. N. Johnson, and T. S. West, Anal. Chim. Acta 57, 281 (1971).

69. R. B. Baird, S. Pourian, and S. M. Gabrielion, Anal. Chem. 44, 1887 (1972).

70. B. M. Patel, R. D. Reeves, R. F. Browner, C. J. Molnar, and J. D. Winefordner, Appl. Spectrosc. 27, 171 (1973).

71. H. M. Donega and T. E. Burgess, Anal. Chem. 42, 1521 (1970).

72. T. Y. Hwang, P. A. Ullucci, and S. B. Smith, Jr., Amer. Lab., August 1971, p. 41.

73. J. Y. Hwang, C. J. Mokeler, and P. A. Ullucci, Anal. Chem. 44, 2019 (1972).

74. T. Takeuchi, M. Yanagisawa, and M. Suzuki, Talanta 19, 465 (1972).

75. M. P. Bratzel, Jr., R. M. Dagnall, and J. D. Winefordner, Appl. Spectrosc. 24, 518 (1970).

76. K. I. Aspila, C. L. Chakrabarti, and M. P. Bratzel, Jr., Anal. Chem. 44, 1718 (1972).

77. C. J. Molnar, R. D. Reeves, and J. D. Winefordner, Appl. Spectrosc. 26, 606 (1972).

78. J. P. Matousek and B. J. Stevens, Clin. Chem. 17, 363 (1971).

79. S. A. Clyburn, B. R. Bartschmid, and C. Veillon, Anal. Chem. 46, 2201 (1974).

80. Pyro-Tech PT-101 Specifications, Ultra Calbon Corporation, P.O. Box 747, Bay City, MI., 48706.

81. W. G. Schrenk and R. T. Everson, Appl. Spectrosc. 29, 41 (1975).

82. C. W. Fuller, Analyst 100, 229 (1975).

83. W. C. Campbell and J. M. Ottaway, Talanta 21, 837 (1974).

84. F. Shaw and J. M. Ottaway, Analyst 100, 217 (1975).

85. C. W. Fuller, Anal. Chim. Acta 62, 442 (1972).

86. M. Williams and E. H. Piepmeier, Anal. Chem. 44, 1342 (1972).

87. S. Yasuda and H. Kakiyama, Bunseki Kagaku 23, 620 (1974).

88. L. H. Ahrens, Spectrochemical Analysis (Addison-Wesley Press, Cambridge, Mass., 1950), pp. 68, 110.

89. W. K. Robbins, Amer. Lab., August 1975, p. 23.

90. N. S. McIntyre, M. G. Cook, and D. G. Boase, Anal. Chem. 46, 1983 (1974).

91. M. D. Amos, Amer. Lab., August 1972, p. 57.

92. M. Yanagisawa and T. Takeuchi, Japan Analyst 23, 364 (1974).

93. J. A. Goleb and C. R. Midkiff, Jr., Appl. Spectrosc. 29, 44 (1975).

94. F. L. Fricke, O. Rose, Jr., and J. A. Caruso, Anal. Chem. 47, 2018 (1975).

95. G. D. Renshaw, Atomic Absorption Newsletter 12, 158 (1973).

96. J. H. Sherfinski, Atomic Absorption Newsletter 14, 26 (1975).

97. G. R. Harrison, R. C. Lord, and J. R. Loofbourow, Practical Spectroscopy (Prentice-Hall, New York, 1941), p. 261.

98. G. F. Larson, V. A. Fassel, R. K. Winge, and R. N. Kniseley, to be published in Appl. Spectrosc.

99. R. A. Sawyer, Experimental Spectroscopy (Prentice-Hall, New York, 1944), pp. 180, 114.

100. C. Duval, Inorganic Thermogravimetric Analysis, 2nd ed., (Elsevier Publishing Co., Amsterdam, 1963), p. 618.

101. R. C. Weast, ed., CRC Handbook of Chemistry and Physics (The Chemical Rubber Co., Cleveland, 1967), pp. B-156, B-187.

102. R. W. Moshier, Analytical Chemistry of Niobium and Tantalum, International Series of Monographs on Analytical Chemistry, Vol. 16, edited by R. Belcher and L. Gordon (Pergamon Press, New York, 1964), p. 15.

103. C. C. Kiess, Natl. Bur. Stds., J. Res. 66A, 111 (1962).

104. J. K. Grime and T. J. Vickers, Anal. Chem. 47, 432 (1975).

105. R. W. B. Pearse and A. G. Gaydon, The Identification of Molecular Spectra, 2nd ed., (John Wiley and Sons, Inc., New York, 1950), p. 36.

106. E. W. Berg, Physical and Chemical Methods of Separation (McGraw-Hill, New York, 1963), pp. 2, 36, 75.

107. J. Korkisch, Modern Methods for the Separation of Rarer Metal Ions (Pergamon Press, Oxford, 1969), p. 357.

108. R. W. Moshier, R. E. Sievers, Gas Chromatography of Metal Chelates (Pergamon Press, Oxford, 1965), p. 42.

109. I. I. Nazarenko, A. N. Ermakov, Analytical Chemistry of Selenium and Tellurium (Halsted Press, New York, 1972), p. 155.

110. R. W. Andrews, Ph.D. thesis, Iowa State University (1975) (unpublished).

111. F. W. E. Strelow, C. J. C. Bothma, Anal. Chem. 39, 595 (1967).

112. V. Schendewolf, Geochim. Cosmochim. Acta 19, 134 (1960).

113. D. F. C. Morris and R. A. Killick, Talanta 10, 279 (1963).

114. C. R. Veale, Analyst 85, 133 (1960).

115. C. R. Veale, J. Inorg. Nuc. Chem. 10, 333 (1959).

116. A. V. Barooshion, M. J. Lautenschleger, and W. G. Harris, Atomlight 71, 5 (1970).

117. A. Iguchi, Bull. Chem. Soc. Japan 31, 748 (1958).

118. A. V. Barooshion, M. L. Lautenschleger, and W. G. Harris, Anal. Biochemistry 42, 281 (1971).

119. S. R. Zimmerley and J. D. Prater, U.S. Patent 2,945,743, July 19, 1960; Chem. Abstr. 54, 20801c (1960).

120. C. E. Mulford, Atomic Absorption Newsletter 5, 88 (1966).

121. W. J. Price, Analytical Atomic Absorption Spectrometry (Heyden and Son, Ltd., London, 1972), pp. 98, 184.

122. T. N. Tweeten and J. W. Knoeck, Anal. Chem. 48, 64 (1976).

123. F. J. Fernandez, Atomic Absorption Newsletter 12, 93 (1973).

124. E. N. Pollock and S. J. West, Atomic Absorption Newsletter 12, 6 (1973).

125. W. Holak, Amer. Lab., August 1974, p. 10.

126. J. A. Fiorino, J. W. Jones and S. G. Capor, Anal. Chem. 48, 120 (1976).

127. F. A. Gooch and A. W. Peirce, Am. J. Sci. 1, Series 4, 181 (1896).

128. J. I. Hoffman and G. C. F. Lundell, Natl. Bur. Stds., J. Res. 22, 465 (1939).

129. W. O. Robinson, H. C. Dudley, K. T. Williams, and H. G. Byers, Ind. Eng. Chem., Anal. Ed. 6, 274 (1934).

130. W. D. Mogerman, Ind. Eng. Chem., Anal. Ed. 33, 307 (1944).

131. J. A. Scherrer, Ind. Eng. Chem., Anal. Ed. 16, 253 (1936).

132. J. A. Scherrer, Ind. Eng. Chem., Anal. Ed. 21, 95 (1938).

133. A. L. Chaney and H. J. Magnuson, Ind. Eng. Chem., Anal. Ed. 12, 691 (1940).

134. F. E. Lichte and R. K. Skogerboe, Anal. Chem. 45, 399 (1973).

135. P.W.J.M. Boumans, F. J. deBoer, F. J. Dahmen, H. Hoelzel, and A. Meier, Spectrochim. Acta 30B, 449 (1975).

136. G. F. Smith, The Wet Chemical Oxidation of Organic Compositions Employing Perchloric Acid (The G. Frederick Smith Chemical Co., Columbus, OH, 1965) p. 36.

137. H. Diehl, Quantitative Analysis (Oakland Street Science Press, Ames, IA, 1970), pp. 91, 315.

138. Certificates of Analysis, Standard Reference Materials (SRM) 1571, 1577, 1630, and 1632, Office of Standard Reference Materials, National Bureau of Standards, U.S. Department of Commerce, Washington, D.C. 20234.

139. K. Liebscher and H. Smith, Arch. Environ. Health 17, 881 (1968).

140. W. H. Allaway, J. Kubota, F. Losee, and M. Roth, Arch. Environ. Health 16, 342 (1968).

141. R. A. Kehoe, J. Cholak, and R. V. Story, J. Nutr. 19, 579 (1940).

142. J. W. Gofman, O. F. deLassa, E. L. Kovick, O. Lowe, W. Martin, D. L. Piluro, R. K. Tardy, and F. Upham, Arch. Environ. Health 8, 105 (1964).

143. R. F. Tarrant and J. Allard, Arch. Environ. Health 24, 277 (1972).

144. P.W.J.M. Boumans and F. J. deBoer, Spectrochim. Acta 30B, 309 (1975).

145. W. Snelleman, T. C. Rains, K. W. Yee, H. D. Cook, and O. Menis, Anal. Chem. 42, 394 (1970).

IX. ACKNOWLEDGMENTS

I wish first to thank Emerson and Helen Nixon for their love and constant encouragement. I wish to also thank Eugene and Carol Catus for their cheerful conversations and many excellent Sunday evening dinners.

Furthermore, the master machinists, glass blowers and medical staff must be acknowledged. The superb workmanship and expertise of Garry Wells, Harry Amenson, Eldon Ness, Tom Johnson, Harold Hall, Evert McKenna, Edgar Moore, and Carol Mack was a major factor in the success of my experimental endeavors.

The guidance and critical review of this work by Dr. Velmer A. Fassel and Dr. R. N. Kniseley is greatly appreciated. I wish to especially thank Dr. Velmer A. Fassel for his critical review of this dissertation and many helpful suggestions for improving my writing style.

The financial support granted to me by Salsbury Laboratories, Charles City, Iowa, is greatly appreciated.

At last, the greatest recognition must be rendered to my lovely wife, Judy -- the long hours spent away from her can never be regained.

X. APPENDIX

Reprinted from ANALYTICAL CHEMISTRY, Vol. 46, Page 75, January 1974

Inductively Coupled Plasma-Optical Emission Analytical Spectrometry

A Compact Facility for Trace Analysis of Solutions

Robert H. Scott,[1] Velmer A. Fassel,[2] Richard N. Kniseley, and David E. Nixon

Ames Laboratory-USAEC and Department of Chemistry, Iowa State University, Ames, Iowa 50010

This paper describes a compact inductively coupled plasma-optical emission system for the trace determination of metallic elements in solution. Theoretical considerations are presented to determine operating parameters which agree well with the empirically determined values. The aerosol desolvation system commonly used with this type of source has been eliminated, and pneumatic nebulization is employed in place of the more elaborate ultrasonic method. Some characteristics of the plasma are reported. Detection limits are in the range 0.1–10 ng/ml for most elements studied. The present facility is readily adaptable to simultaneous multielement trace analysis.

The use of inductively coupled plasmas as excitation sources for trace metal determinations was first investigated independently by Greenfield and associates (*1*) and by Wendt and Fassel (*2*) after Reed's pioneering work in the field of radiofrequency plasma generation (*3-5*). Several authors have subsequently demonstrated the feasibility of this technique in emission spectrometry (*6-22*). Most of these investigations were performed with available equipment in the form of rather large radiofrequency heating devices (*2, 8, 12, 14, 15, 18-20, 22*). These reports have occasionally created the misleading impression that the technique is inherently impractical and costly. The high power capacity of the generators, the large argon consumption rates used, and the difficulty sometimes experienced in coupling the radiofrequency energy into the plasma under varying conditions also have contributed to the above impression.

Recent technological developments and experimental findings have made it possible to assemble and evaluate a compact system specifically designed to fulfill the requirements of a practical, viable analytical technique. The system described in this communication possesses the following desirable hardware and operational features: a compact table model radiofrequency generator (dimensions 90 × 50 × 30 cm); well designed impedance matching circuitry and plasma tube configuration for instantaneous ignition and stable operation of the plasma; low argon consumption rate (~10 l./min) resulting in an operating cost comparable to that of a conventional nitrous oxide-acetylene flame used in atomic absorption spectrometry; elimination of the aerosol desolvation system; and replacement of the more elaborate ultrasonic nebulization system with a pneumatic nebulizer.

Plasma Operating Parameters. The inductively coupled, argon-supported plasma used in the present study is formed in a vertical quartz tube configuration surrounded longitudinally by a two-turn coil carrying an oscillating current. The oscillating magnetic field generates eddy currents in the plasma which flow in closed circles in planes perpendicular to the coil axis. These induced currents encounter resistance to their flow resulting in Joule heating. Sample aerosol is injected into the center of the plasma along the axis (*1, 16, 23*). The theoretical determination of operating parameters is based on the requirements of a high coupling efficiency of radiofrequency power into the argon plasma and efficient heating of the injected sample aerosol to a desirable temperature.

To calculate the optimum relationship between the frequency and plasma radius, we shall assume that the plasma behaves similar to a metallic cylinder of constant electrical conductivity (*24*). The total power absorbed and the coupling efficiency can then be described by a Bessel function of the ratio r/s where r is the plasma radius and s is a quantity known as the skin depth, which is the depth in the plasma at which the induced annular current density is $1/e$ of the surface value (*24-26*). The function relating the coupling efficiency and r/s is given in Ref. (*25*). When this function is plotted *vs.* r/s, a knee appears in the curve at about $r/s = 2.25$. For greater values, the coupling efficiency does not increase significantly. For efficient heating of the injected aerosol along the plasma axis, it is desirable that r/s should be as small as possible, and therefore a value of 2.25 is considered optimal.

The skin depth is given by the well known relationship

$$s(\text{cm}) = 5.03/\sqrt{\mu\sigma\nu} \qquad (1)$$

where μ is the relative permeability and σ is the specific electrical conductivity (Ω^{-1} cm^{-1}) of the absorbing medium, and ν is the frequency of the electromagnetic field (MHz).

The desired relationship between the frequency and plasma radius is obtained by setting $r/s = 2.25$ in Equation 1, giving

$$\nu r^2 = 128/\mu\sigma \qquad (2)$$

For gases, μ can be taken as unity and σ is a function of the temperature and pressure. The function $\sigma(T)$ for argon at atmospheric pressure is shown in Figure 1 (*24, 27*). From Equation 2 and Figure 1 the relationship between temperature and frequency for various optimized plasma radii can be obtained, as shown in Figure 2.

The temperature in the eddy current region is a function of the radiofrequency power input and the flow characteristics of the argon. The enthalpy of the argon after passing through the region in which the power is transferred is given by

$$H = \int C_p dT \qquad (3)$$

where C_p is the heat capacity at constant pressure (cal/mol. K) and T is the temperature of the heated gas. For argon at atmospheric pressure and $T < 10{,}000$ K, C_p is equal to $5/2\ R$, where R is the gas constant (1.986 cal/mol K). If the argon is introduced into the system at a flow-rate of ϕ l./min, the power required to heat all of the gas to a temperature T is given by

$$P(\text{W}) = 0.015\ \phi T \qquad (4)$$

The above temperature, for the sake of simplicity, may be considered as an "average" gas temperature. It is obvious that the heated argon will have a radial temperature distribution which will change with height above the load

[1]Present address, National Physical Research Laboratory, Council for Scientific and Industrial Research, Pretoria, South Africa.
[2]To whom requests for reprints should be sent.

(1) S. Greenfield, I. L. Jones, and C. T. Berry, *Analyst (London)*, **89**, 713 (1964).
(2) R. H. Wendt and V. A. Fassel, *Anal. Chem.*, **37**, 920 (1965).
(3) T. B. Reed, *J. Appl. Phys.*, **32**, 821 (1961).
(4) T. B. Reed, *Int. Sci. Technol.*, **6**, 42 (1962).
(5) T. B. Reed, *Proc. Nat. Electron. Conf.*, **19**, 654 (1963).
(6) S. Greenfield, *Proc. Soc. Anal. Chem.*, **2**, 111 (1965).
(7) H. Dunken and G. Pforr, *Z. Chem.*, **6**, 278 (1966).
(8) M. E. Britske, V. M. Borisov, and Yu. S. Sukach, *Zavod. Lab.*, **33**, 252 (1967).
(9) H. C. Hoare and R. A. Mostyn, *Anal. Chem.*, **39**, 1153 (1967).
(10) V. A. Fassel and G. W. Dickinson, *Anal. Chem.*, **40**, 247 (1968).
(11) W. Barnett and V. A. Fassel, *Spectrochim. Acta, Part B*, **25**, 139 (1970).
(12) C. Veillon and M. Margoshes, *Spectrochim. Acta, Part B*, **23**, 503 (1968).
(13) G. Pforr, "Proceedings of the XIV Colloquium Spectroscopium Internationale," Adam Hilger, London, 1968, p 687.
(14) J. M. Mermet and J. Robin, "Proceedings of the XIV Colloquium Spectroscopium Internationale," Adam Hilger, London, 1968, p 715.
(15) V. M. Goldfarb, V. H. Golkhman, and V. Kh. Golkhman, *Zh. Prikl. Spektrosk.*, **8**, 193 (1968).
(16) G. W. Dickinson and V. A. Fassel, *Anal. Chem.*, **41**, 1021 (1969).
(17) G. Pforr and O. Aribot, *Z. Chem.*, **10**, 78 (1970).
(18) D. Truitt and J. W. Robinson, *Anal. Chim. Acta*, **49**, 401 (1970).
(19) G. H. Morrison and Y. Talmi, *Anal. Chem.*, **42**, 809 (1970).
(20) S. Greenfield and P. B. Smith, *Anal. Chim. Acta*, **59**, 341 (1972).
(21) P. W. J. M. Boumans and F. J. de Boer, *Spectrochim. Acta, Part B*, **27**, 391 (1972).
(22) G. F. Kirkbright, A. F. Ward, and T. S. West, *Anal. Chim. Acta*, **62**, 241 (1972).
(23) V. A. Fassel, "Electrical Flame Spectroscopy," XVI *Colloquium* Spectroscopium Internationale, Plenary Lecture, Reprint, Adam Hilger, London, 1972, p 63.
(24) Yu. P. Raizer, *Sov. Phys. Uspekhi.*, **12**, 777 (1970).
(25) A. Mironer and F. Hushfar, "Radio Frequency Heating of a Dense Moving Plasma," *Preprint 63045-63*, unpublished paper presented at AIAA Electric Propulsion Conference, Colorado Springs, Colo., March 1963.
(26) G. W. Dickinson, Ph.D. thesis, Iowa State University, Ames, Iowa, 1969.
(27) S. C. Lin, E. L. Resler, and A. Kantrowitz, *J. Appl. Phys.*, **26**, 95 (1955).

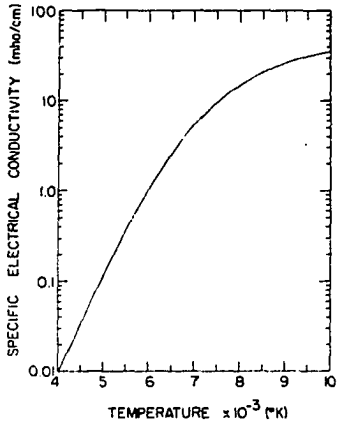

Figure 1. Specific electrical conductivity of argon at various temperatures (24,27)

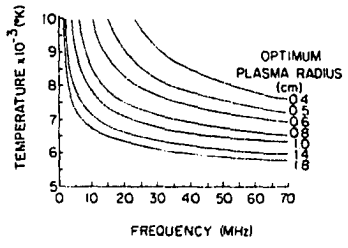

Figure 2. Optimum plasma radius as a function of frequency and plasma temperature in eddy current region

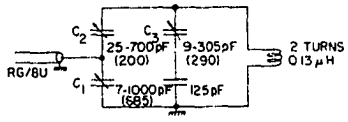

Figure 3. Diagram of coupling circuit

coil because of radiation and conduction losses and expansion processes. This radial temperature distribution, therefore, is a complex function of the radiofrequency power absorption and gas flow characteristics and is difficult to calculate. The gas flow characteristics are primarily determined by the practical requirement of containing the high temperature plasma inside the load coil by means of a fused quartz tube. A method of cooling the tube wall is essential or else the close proximity of the plasma will cause the wall to melt. When the vortex stabilization technique devised by Reed (4) is employed, the argon is introduced tangentially, resulting in a spiral flow up the tube with a low pressure region toward the center. The high flow velocity of argon along the wall then tends to keep the plasma centered and away from the wall. This technique places a practical lower limit to the argon flow rate necessary to prevent the quartz tube from overheating.

In Figure 2, it is seen that for a frequency of 27 MHz and a plasma radius of 0.8 cm, a temperature of about 7250 K should be produced in the eddy current region for efficient coupling. This temperature is in principle determined by the available power (Equation 4). The plasma radius is governed by the radial dimensions of the plasma tube configuration. Our efforts to employ smaller radii than that above were met with temperature stability problems and greater difficulty in injecting the aerosol into the plasma. A plasma radius of about 0.8 cm was an acceptable compromise.

The efficiency of coupling the radiofrequency power into the plasma is dependent on the impedance match between the plasma and the transmission line carrying the power from the generator. To estimate the resistive impedance of the plasma, we again assume a behavior similar to a metallic cylinder. For this behavior, the impedance is approximately given by

$$R_p(\Omega) = l / A\sigma \qquad (5)$$

where l is equal to the length of the "unfolded" eddy current region, given by $\pi(2r - s)$, and A is the cross sectional area of this region given by hs, where h is the height of the region (cm). For $r/s = 2.25$, we obtain

$$R_p = 3.5\,\pi / h\sigma \qquad (6)$$

For a temperature in the eddy current region of 7000 to 8000 K and for $h \approx 1.5$ cm, $R_p \approx 0.5$ to 1.5 ohms. This impedance is transformed to 2 to 6 ohms for a two-turn load coil in the case of no coupling losses. Because the transmission line impedance in the present design is 50 Ω, an adjustable impedance matching circuit (coupling unit) is necessary between the transmission line and the load coil. This circuit is described in the following section.

Table I. Plasma Operating Parameters

Frequency	27 MHz
Net radio frequency power input to coupling unit	1 kW
Argon coolant flow rate	10 l./min
Argon flow rate for aerosol transport	1.4 l./min
Aerosol flow rate to plasma	~0.1 ml./min
Specific electrical conductivity of argon plasma in eddy current region (approx.)	10 Ω^{-1} cm^{-1}
Skin depth (approx.)	0.3 cm
Plasma radius (approx.)	0.8 cm

The plasma operating parameters chosen for the present study are given in Table I. Although the net power input, gas flow rates, and plasma radius were determined more on an empirical basis, the above theoretical approach yields results which are in good agreement with the experimentally defined values. We admit that in our theoretical treatment we chose values for parameters such as r/s and the electrical conductivity of the plasma on a somewhat arbitrary but realistic basis. Thus, it is quite possible that these values could have been manipulated somewhat and still obtain eventual agreement with the experimentally defined operating parameters shown in Table I.

EXPERIMENTAL FACILITIES AND PROCEDURES

Radiofrequency Generator. The radiofrequency generator (International Plasma Corporation, Hayward, Calif. 94544) consists of a crystal controlled oscillator and air-cooled power amplifier. The oscillation frequency is 27.12 MHz. The power output is adjustable to a maximum of 2 kW. Both forward and reflected power can be monitored on a built-in meter. Power is fed via a coaxial cable (type RG-8U) to a coupling unit which houses the variable capacitors for matching the plasma load to the transmission line. The output coil is mounted on the front of the coupling unit and an accurately machined Bakelite clamp supports and centers the plasma tube configuration inside the coil. To reduce radiofrequency interference with other instrumentation, the assembly is enclosed in a metal housing secured to the front end of the coupling unit.

Coupling Unit. A diagram of the coupling circuit (International Plasma Corporation, Hayward, Calif. 94544) is shown in Figure 3. Variable (30-turn) vacuum capacitors are used because of their greater stability. The two-turn water-cooled load coil is fabricated

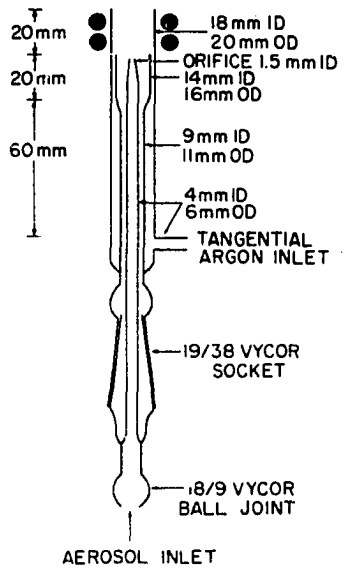

Figure 4. Diagram of plasma tube configuration

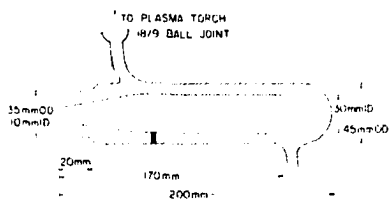

Figure 5. Diagram of dual tube sample chamber

of 5-mm o.d. copper tubing. The coil diameter is ~3 cm and the centerline to centerline spacing is 8 mm. The calculated inductance is 0.13 μH excluding the stray inductance caused by the mounting leads. The coupling unit is mounted on a stand which permits its horizontal and vertical adjustment.

Plasma Tube Configuration. The concentric quartz tube configuration, hereafter called the torch, is similar to that described previously (23) except that no "plasma gas" is used in the present design. A schematic diagram of the torch is shown in Figure 4. The torch is fabricated of fused quartz tubing and consists of concentric outer and inner tubes (called the coolant and plasma tube, respectively) and a removable aerosol injection tube. Argon is introduced tangentially through a side tube. The argon flow velocity is caused to increase toward the top of the plasma tube by the constriction, resulting in an increase in both the cooling efficiency and the degree of vortex stabilization. The optimum constriction width has been empirically determined to be 1 mm for the present system. A larger spacing (2 mm) necessitated a higher argon consumption rate because of inefficient cooling of the outer tube wall, whereas a smaller spacing (0.5 mm) resulted in plasma instability.

The diameter of the orifice of the aerosol injection tube was also optimized empirically. For a constant argon flow rate through the orifice, the injection velocity of the aerosol into the plasma is inversely proportional to the square of the orifice diameter. If the injection velocity is too low, the aerosol will not penetrate the "doughnut hole" of the plasma (16, 23). If the injection velocity is too high, the residence time of the particles will be unfavorably short. An orifice diameter of 1.5 mm and an argon flow rate of about 1.4 l./min were acceptable compromises of these parameters. Assuming that the velocity of the particles remains constant and equal to the injection velocity (which is approximately 1300 cm sec^{-1} for the above parameters), the particle residence time is approximately 2.5 msec for an observation height of 18 mm above the load coil.

Because the aerosol is injected into the "doughnut hole" of the plasma and since most of the radiofrequency power is absorbed in the "doughnut" (*i.e.*, within the skin depth), the aerosol is principally heated by conduction and radiation from the surrounding argon. This indirect heating process is favorable because major changes in sample composition would not be expected to change the absorbed power significantly.

Table II. Spectrometric Instrumentation

Spectrometer:	
Ebert mount, 0.5-m	0.5-m focal length (Jarrell-Ash Division, Fisher Scientific Co., Waltham, Mass., Model No. 82000)
Fixed slits	50-μm entrance 50-μm exit
Grating	1160 rulings/mm, blazed at 2500 Å, first order
Reciprocal linear dispersion	16 Å/mm, first order
Photomultiplier	EMI 6256B, S-13 response
Optics:	
Plasma imaged in 1:1 ratio onto entrance slit using 15-cm focal length × 5-cm diameter fused quartz lens	
Amplifier:	
Linear picoammeter with remote pre-amplifier and built-in zero suppression (Keithley Instruments, Cleveland, Ohio, Model No. 417)	
Recorder:	
X-Y recorder (Moseley Division, Hewlett-Packard, Pasadena, Calif., Model No. 7001A)	
Integrator:	
Digital readout system (Infotronics, Houston, Texas, Model No. CRS-80).	

Nebulizer and Aerosol Chamber. A right-angle pneumatic nebulizer was used with a solution uptake rate of 3.0 ml/min for an argon flowrate of 1.4 l./min at 27.5×10^4 Nm $^{-2}$. Details of the construction of this nebulizer are given in Ref. (28).

To reduce random fluctuations in signal intensity commonly caused by the process of pneumatic aerosol generation, a dual-tube aerosol chamber was devised. A schematic diagram is shown in Figure 5. The purpose of the central tube is to separate the forward and reverse aerosol flows, the latter produced as a result of the low pressure in the region of high aerosol velocity. The turbulence within the chamber is reduced and less condensation occurs on the nebulizer, resulting in a reduction in the signal noise in the plasma. The aerosol is fed directly to the plasma. No external desolvation apparatus [*e.g.*, Ref. (29)] is used. The rate at which the aerosol entered the plasma was ~0.1 ml of solution per minute for an argon flow rate of 1.4 l./min. This was derived by measuring the difference between the volume of runoff solution and uptake over a period of 1 hour. The efficiency of the nebulizer is therefore ~3%.

Spectrometer and Readout System. The results reported in this paper were obtained with the instrumentation described in Table II. Simultaneous multielement analyses with a 30-channel spectrometer are presently under way. The results obtained under multichannel conditions do not differ significantly from those obtained separately with the single channel system (30).

Plasma Generation. The plasma is generated by first flushing the sample chamber and torch with argon and then touching the quartz tube near the coil with a Tesla coil to ionize the argon. It is important to stop the aerosol flow during this operation, while maintaining a coolant flow rate of approximately 10 l./min. Since the "Tesla-ionized" argon has a higher impedance than the final plasma, it is necessary to adjust the capacitors in the coupling unit until the impedance of the ionized argon is approximately matched to the transmission line. At this point, sufficient radiofrequency power will couple into the ionized argon to form a stable plasma. The capacitors should then be readjusted until a minimum reflected power is indicated on the power meter. The aerosol is then introduced, resulting in a visible axial passage in the plasma as seen in Figure 6.

(28) R. N. Kniseley, H. Amenson, C. C. Butler, and V. A. Fassel, unpublished data, Ames Laboratory—USAEC and Department of Chemistry, Iowa State University, Ames, Iowa 50010 (1972).
(29) C. Veillon and M. Margoshes, *Spectrochim. Acta, Part B*, 23, 553 (1968).
(30) R. Winge, R. N. Kniseley, V. A. Fassel, and W. Sutherland, unpublished data.

Figure 6. Photograph of inductively coupled plasma to show aerosol channel through plasma center

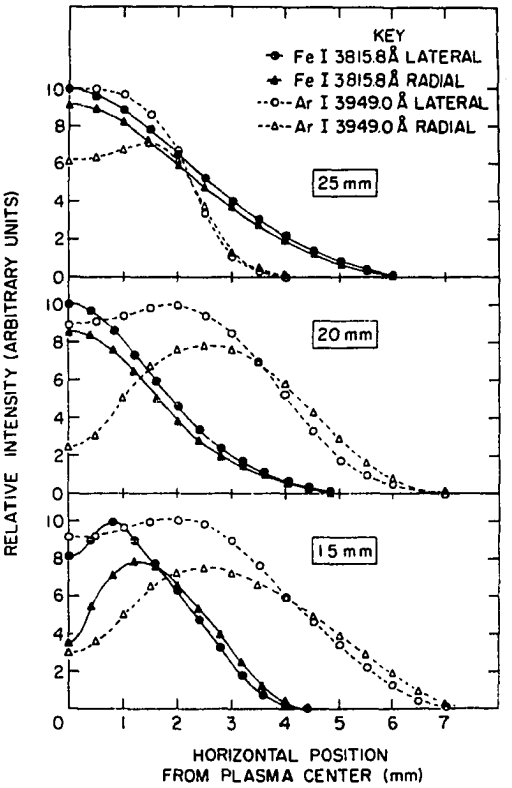

Figure 7. Normalized relative intensities of the Fe line at 3815.8 Å and Ar line at 3949.0 Å as a function of the horizontal position from the plasma center for various heights above the load coil. Both lateral intensities (measured) and radial intensities (calculated by the Abel inversion technique) are shown

Difficulty in generating the plasma may be due to incorrect settings of C_1, C_2, and C_3 (Figure 3). In this case, initial tuning may be achieved with a dummy load consisting of a 50-100 W filament-type light bulb shorted by a loop of insulated wire, which is loosely inductively coupled to the load coil. As the capacitors are adjusted toward the proper settings, the lamp will glow. Eventually the radiofrequency power input must be reduced to avoid melting of the lamp filament. The capacitors should be adjusted until maximum lamp brightness is reached. These settings will be close to the correct values for generating the plasma as described above. Once the plasma has been generated and properly tuned, it is easily regenerated after extinguishment by applying the Tesla coil as described and slowly reducing the capacitance of C_2 (Figure 3) by about 10 pf (half-turn). When the ionized argon ignites, C_2 should be returned to its original setting. If difficulty in generating the plasma persists, it may be necessary to increase the coolant flowrate to 15 l./min or more during the ignition period.

A coolant flowrate of 10 l./min is sufficient for a net power input of up to 1.3 kW when the concentric quartz tube components are properly aligned and the torch assembly is accurately centered in the coil. Misalignment will cause overheating because of inadequate cooling of the outer tube wall in the region of the lower flow velocity. To prevent damage to the tube in this instance, it is necessary to increase the coolant flow rate or decrease the power input, both resulting in a decrease in plasma temperature. If the plasma tube or aerosol tube overheats, the height of the torch relative to the load coil should be reduced. In the present set-up, a 1-2 mm gap between the top of the plasma tube and the base of the load coil has proved satisfactory.

When highly concentrated salt solutions are nebulized, desolvated aerosol droplets may coalesce at the injection orifice of the aerosol tube, resulting in instability in the injection process. This occurs, for example, after approximately 1 hour of continuous nebulization of solutions containing ~1 wt % Fe^{3+}. The rate of coalescence can be reduced by lowering the aerosol injection tube with respect to the plasma but this may lead to difficulty in injecting the aerosol into the plasma center. Notwithstanding the above, under normal operation with solutions containing up to 0.5% dissolved analyte, the torch can be operated over periods up to several days before cleaning is necessary. This is simply effected with the aid of a pipe cleaner without having to dismantle the torch.

RESULTS AND DISCUSSION

Assuming that the plasma is in local thermal equilibrium (*31*, *32*), preliminary temperature measurements for a plasma generated with a power input of 1 kW, an argon coolant flow rate of 10 l./min and an argon (aerosol) flow rate of 1.4 l./min gave a temperature in the aerosol channel of about 5000 K at a height of 18 mm above the load coil. Temperatures of about 6500 K were measured lower down in the plasma in the off-axis region just above the load coil (*33*).

The horizontal spectral line profiles of Fe I 3815.8 Å (4.7 eV) and Ar I 3949.0 Å (14.7 eV) for various heights above the load coil are shown in Figure 7. Both the lateral (measured) and radial (calculated) intensities are shown. The radial intensity profiles were calculated from the measured profiles using the inversion technique of Cremars and Birkebak (*34*). The lower axial iron and argon line intensities at an observation height of 15 mm imply a lower

(31) P. D. Scholz and T. P. Anderson, *J. Quant. Spectrosc. Radiat. Transfer*, **8**, 1411 (1968).
(32) A. D. Stokes, *J. Phys. D: Appl. Phys.*, **4**, 916 (1971).
(33) D. Kalnicky, unpublished data, Ames Laboratory-USAEC and Department of Chemistry, Iowa State University, Ames, Iowa 50010 (1972).
(34) C. J. Cremars and R. C. Birkebak, *Appl. Opt.*, **5**, 1057 (1966).

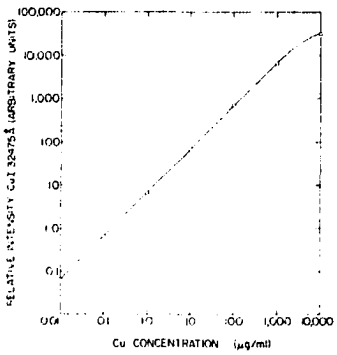

Figure 8. Analytical curve obtained for Cu 3247.5 Å. Observation height was 18 mm

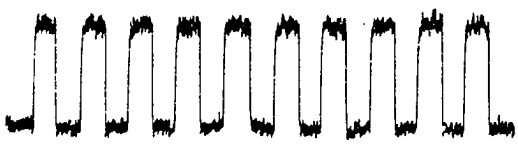

Figure 9. Signals obtained for Pb 4057.8 Å for a solution containing 0.2 μg/ml Pb. Analyte and blank solutions were run alternately at 1-minute intervals

temperature in the aerosol channel than in the surrounding region, which is not unexpected because the highest temperature is found in the eddy current region. There is sufficient reason to assume that the radial temperature profile has similar shape to that of the argon line intensity. Because the aerosol is injected into the plasma in a comparatively narrow central channel, the decrease in the Fe line intensity in the horizontal direction is due to a decrease in the number density of the Fe atoms rather than a decrease in temperature.

Evidence of negligible self-absorption of analyte spectral line emission in the axial channel is given in Figure 8, which shows a typical analytical curve extending linearly over a five-decade concentration range, even though a resonance line was used. These data signify that the source remains optically thin at 3247.5 Å up to several orders of magnitude above the detection limit when the resolution of the observing instrument is several times the line width.

Because of the higher temperature environment in these plasmas as compared to commonly used combustion flames, "chemical" or solute vaporization type interferences do not occur to the degree observed in conventional flames (*1*, *25*). However, a possible disadvantage of the higher temperature is the associated high degree of ionization of easily ionizable elements. The presence of easily ionizable concomitants may influence the ionization equilibrium of the sample. The extent of this ionization interference is presently being studied and will be discussed in detail in a future publication.

Detection Limits. Table III gives the detection limits obtained for a number of elements at an observation height of 18 mm above the load coil. The best values reported for flame atomic absorption and fluorescence are also listed. The present detection limits represent the concentration of each analyte in solution necessary to increase the measured signal by twice the standard deviation of the blank signal at the wavelength of the analysis line. The values were calculated from the measured signal-to-noise ratios at analyte concentrations of 0.1 μg/ml. For most elements, the detection limits did not change significantly as the observation height was varied between 15 mm and 25 mm above the load coil for reasons given in Ref. (*21*) even though a change in the signal to background occurred. Therefore, the height at which the maximum signal-to-background ratio occurred was not necessarily the height associated with the lowest detection limit.

Table III. Typical Detection Limits, μg/ml

Element and spectral line,[a] Å	Excitation potential, eV	Plasma	Flame atomic absorption (*35*)	Flame atomic fluorescence (*35*)
Al I 3961.5	3.1	0.001	0.1	50.
Ba II 4554.0	2.7	0.0001	0.05	...
Ca II 3933.7	3.2	0.0005	0.002	0.02
Co I 3453.5	4.0	0.004	0.005	0.01
Cr I 4254.3	2.9	0.001	0.005	0.05
Ni I 3414.8	3.6	0.003	0.005	0.003
Pb I 4057.8	4.4	0.008	0.01	0.01
Se I 1960.3	6.5	0.1	0.1	1.0
Ti II 3349.0	4.3	0.005	0.1	...
V I 4379.2	3.1	0.002	0.02	...
Y II 3710.3	3.5	0.0006	0.3	...
Zn I 2138.6	5.8	0.01	0.002	0.00004

[a] Used in present study.

The values reported in Table III are similar to those reported in Ref. (*23*), but are somewhat higher than those reported by Boumans and de Boer (*21*). However, experimental parameters, such as height of observation and aerosol flow rate, were not optimized for each element as was done in Ref. (*21*) because one of the main advantages of the present technique is the ability to determine a number of elements simultaneously when a multichannel spectrometer is used.

The stability of the entire system is represented in Figure 9, which shows alternate 1-minute recordings of the signal at 4057.8 Å for a solution containing 0.2 μg/ml Pb and a blank solution. The overall amplifier/recorder time constant was 600 msec. Each signal was recorded and integrated simultaneously with an integration period of 16 sec. The calculated relative standard deviation of the net signal, *i.e.*, the measuring precision, was 0.6%.

CONCLUSION

The results obtained in this study emphasize the potential of an inductively coupled plasma as an excitation source for simultaneous multielement analysis at concentration levels equal to or lower than those achievable by conventional flame atomic absorption or fluorescence techniques. The method has been simplified by the use of pneumatic nebulization rather than more elaborate ultrasonic nebulization and the elimination of an external aerosol desolvation apparatus, which has a slower response and is more liable to memory effects (*21*). Furthermore, the relatively low radiofrequency power and argon consumption rates are favorable economic factors.

Received for review April 5, 1973. Accepted July 19, 1973.

(35) J. D. Winefordner, V. Svoboda, and L. J. Cline, *Crit. Rev. Anal. Chem.*, August 1970, pp 233–274.